General Disclaimer

One or more of the Following Statements may affect this Document

- This document has been reproduced from the best copy furnished by the organizational source. It is being released in the interest of making available as much information as possible.

- This document may contain data, which exceeds the sheet parameters. It was furnished in this condition by the organizational source and is the best copy available.

- This document may contain tone-on-tone or color graphs, charts and/or pictures, which have been reproduced in black and white.

- This document is paginated as submitted by the original source.

- Portions of this document are not fully legible due to the historical nature of some of the material. However, it is the best reproduction available from the original submission.

Produced by the NASA Center for Aerospace Information (CASI)

CR-137968

Princeton University

(NASA-CR-137968) AN EXPERIMENTAL STUDY OF THE NONLINEAR STIFFNESS OF A ROTOR BLADE UNDERGOING FLAP, LAG AND TWIST DEFORMATIONS Final Technical Report (Princeton Univ., N.J.) 58 p HC A04/MF A01 CSCL 01A G3/02

N77-10008

Unclas 08056

NOV 1976
RECEIVED
NASA STI FACILITY
INPUT BRANCH

Department of
Aerospace and
Mechanical Sciences

CR-137968

AN EXPERIMENTAL STUDY OF THE NONLINEAR STIFFNESS OF A ROTOR BLADE UNDERGOING FLAP, LAG AND TWIST DEFORMATIONS

by
E. H. Dowell
and
J. Traybar

AMS Report No. 1194

January 1975

prepared for
U.S. ARMY AIR MOBILITY RESEARCH AND DEVELOPMENT LABORATORY
Ames Research Center

Contract NAS 2-7615

FOREWORD

This final technical report was prepared by the Aeroelasticity and Flight Mechanics Laboratories of the Department of Aerospace and Mechanical Sciences, Princeton University, Princeton, New Jersey under Contract number NAS 2-7615 with NASA-Ames Research Center. It was funded by and under the technical direction of the U.S. Army Air Mobility Research and Development Laboratory, Ames Directorate, Ames Research Center at Moffett Field, California and was monitored and administered by Dr. Dewey H. Hodges of that directorate.

The work covered in this report was supervised and performed by Professor E. H. Dowell, Principal Investigator. He was aided in the experiments by Mr. Joseph J. Traybar, Research Staff and Mr. J. P. Kukon, Technical Staff. The test equipment and apparatus was fabricated by Messrs. E. L. Griffith and J. A. Grieb., Specialists.

For internal control the Aerospace and Mechanical Sciences Department has designated this work as AMS Report Number 1194.

ABSTRACT

An experimental study of the large deformation of a cantilevered beam under a gravity tip load has been undertaken. The beam root is rotated so that the tip load is oriented at various angles with respect to the beam principal axes. Static twist and bending deflections of the tip and bending natural frequencies have been measured as a function of tip load magnitude and orientation. The experimental data are compared with the results of a recently developed non-linear structural theory and agreement is good for deflections small compared to the beam span with systematic deviations for larger deflections. These results support the validity and utility of the nonlinear structural theory for rotor blade applications.

TABLE OF CONTENTS

FOREWORD	i
ABSTRACT	ii
LIST OF FIGURES AND TABLES	iv
LIST OF SYMBOLS	v
INTRODUCTION	1
EXPERIMENTAL APPARATUS AND METHODS	3
THEORETICAL MODEL	7
EXPERIMENTAL RESULTS AND COMPARISON WITH THEORY	11
CONCLUSIONS AND RECOMMENDATIONS	15
REFERENCES	51

LIST OF FIGURES AND TABLES

Figure number		Page
2.1	Photograph of Apparatus and Set-up for Static Deflection Experiments Showing Loaded and Unloaded Conditions.	16
2.2	Photograph of Apparatus and Set-up for Frequency Measurement Experiments Showing Steady and Oscillating Conditions.	17
2.3	Axis System and Notation	18
2.4	Schematic Showing Typical Loading Procedures and Excitation/ Deflection Sense	19
2.5	Static Deflection of Blade Tip Elastic-Axis Reference Point with Applied Load for Several Pitch Angles	20
2.6	Typical Segment of Recording-Oscillograph Chart for Frequency Data	21
4.1	Geometry	22
4.2	Deflection vs Load $\theta = 90^{\circ}$, $\theta = 0^{\circ}$	23
4.3	Deflection vs Load $\theta = 30^{\circ}$	24
4.4A	Deflection vs Load $\theta = 30^{\circ}$, Flapwise Deflection	25
4.4B	Deflection vs Load $\theta = 30^{\circ}$, Chordwise Deflection	26
4.5	Deflection vs Load $\theta = 40^{\circ}$	27
4.6	Deflection vs Load $\theta = 30^{\circ}$	28
4.7	Deflection vs Load $\theta = 50^{\circ}$	29
4.8	Natural Frequency vs Dead Weight Loading Orientation-Experimental	30
4.9	Natural Frequencies vs Dead Weight Loading Orientation Theoretical, FF = 1.0	31
4.10	Natural Frequencies vs Pitch Angle, P = 1 lb Tip Weight	32
4.11	Natural Frequencies vs Pitch Angle, P = 2 lb Tip Weight	33
4.12	Natural Frequencies vs Pitch Angle; Various Tip Weights	34
4.13	Natural Frequencies vs Pitch Angle, P = 1 lb Tip Weight	35
4.14	Natural Frequencies vs Pitch Angle, P = 2 lb Tip Weight	36
4.15	Natural Frequencies vs Pitch Angle; Various Tip Weights	37
4.16	Natural Frequencies vs Tip Weight $\theta = 0^{\circ}$	38
4.17	Natural Frequencies vs Tip Weight $\theta = 0^{\circ}$	39
Table I	Test 51: Blade Frequency Experiments using Aluminum Beam: Radius = 20"	40
Table II	Test 52: Blade Frequency Experiments using Aluminum Beam: Radius 30"	46

LIST OF SYMBOLS

b	- rotor blade (beam) width
D	- stiffness parameter; see equation (4), et. seq.
$EI_{y'}$, $EI_{z'}$	- lag, flap bending stiffnesses
e	- $EI_{z'}/EI_{y'}$
f	- frequency
GJ	- torsional stiffness
g	- gravitational constant; also $GJ/EI_{y'}$
h	- rotor blade thickness
K_{111}	- modal constant
m	- beam mass/per unit span
M_{TIP}	- tip mass
$\underline{P}$	- gravity tip load; = $M_{TIP}g$
R	- rotor blade span
v	- lag (chordwise) bending deflection
w	- flap bending deflection, $\underline{1}$ to v
x	- spanwise coordinate
β_1, γ_1	- modal constant
ψ_1	- assumed bending mode shape
θ	- angle between rotor blade chord and vertical (pitch angle)
μ_o	- mass parameter; see equation (4) et. seq.

Subscripts

1 - first mode

Superscripts

$' \equiv \frac{d}{dt}\left(\frac{mR^4}{EI_{y'}}\right)^{1/2}$

o - static equilibrium

^ - dynamic perturbation

Additional Notation

≡ pounds

1. INTRODUCTION

Hodges and Dowell[1,2] have formulated a nonlinear theory of hingeless rotor blade dynamics which indicates that the primary nonlinear effect is due to a nonlinear stiffness arising from mutual interaction among elastic flap, lag and twist. The goal of the present study has been to devise a simple experiment to measure the predicted effect and make a quantitative comparison of the results with the theoretical model.

The simplest relevant experiment would appear to be a non-rotating uniform beam under a static point load. A measurement of the variation of static deflections in flap, lag (and twist) and also flap and lag natural frequencies with static load allows an evaluation of the theory. A strictly linear model would predict a linear variation of flap and lag static deflections with load and no twist. Also a linear model would predict no change in natural frequencies with static load. On the other hand, the Hodges-Dowell nonlinear model predicts nonlinear variations of static flap, lag and twist deflection with static load and a change in natural flap and lag natural frequencies with load. Hence, the proposed experiment does provide a critical test of the nonlinear theory.

How to provide a static point force to the beam without introducing additional dynamic effects is a delicate question, however. For example, if one uses a weight and gravity to provide the force, its inertial mass would also change directly the dynamic characteristics of the rotor blade. Similarly, for a spring induced static force, dynamic effects are

inevitably introduced as well. In principle for a relatively long, heavy, flexible beam the mass effect may be made as small as desired. Conversely, for a relatively short, stiff beam and a relatively long, soft spring the dynamic effect of the spring may be made as small as desired. In practice neither option leads to rotor blades (beams) of convenient dimensions. Hence, we have chosen to use a gravitational force and incorporate the inertial effects of the weight in our mathematical model. The latter, though quantitatively substantial, are nevertheless non-controversial and readily accounted for theoretically. To make the experiment as simple as possible a tip weight was used whose dimensions are small relative to the radius of the uniform, rectangular cross-section rotor blade. Hence, the torsional frequency is substantially higher (greater than a factor of ten) than either the flap or lag frequencies. In the following, the experimental apparatus and method is described in some detail. Next, the theoretical method is briefly reviewed and the experimental data are presented and compared with the available theory. Finally, conclusions are drawn and recommendations for further work made.

2. EXPERIMENTAL APPARATUS AND METHODS

Experimental Apparatus

Photographs of the experimental apparatus are shown in Fig. 2.1 and 2.2.

In the experimental phase of the study, blade spars were simulated by various sized rectangular sections fabricated from 7075 aluminum. The 7075 aluminum belongs to a zinc alloy group noted for its very high strength and hardness. The typical mechanical properties are:

Modulus of elasticity; 10.4×10^6 psi

Tension strength; Ultimate, 83,000 psi; yield 73,000 psi

Shearing strength; 48,000 psi

All beams were machined from 7075 aluminum stock with the temper designation 651 where coded number 6 defines the basic temper, coded number 5 denotes that the material has received stress relieval treatment and the coded number 1 indicates the method used to effect stress relief -- in this case "stretching". All beams were carefully machined to size so that machining stresses, warping and bending were minimized. The beams fabricated for these experiments were sized as indicated below:

Beam #1: Length (Radius) 20", Width 1", Thickness 1/8"

Beam #2: Length (Radius) 20", Width 1/2", Thickness 1/8"

Beam #3: Length (Radius) 30", Width 1/2", Thickness 1/8"

Beams 2 and 3 were instrumented with strain gages mounted at the roots on the width and thickness portions of the beam. These gages were mounted in the proper orientation to be utilized as frequency transducers (combined with the associated signal conditioning instrumentation) to measure chordwise and flapwise beam natural frequencies accurately. All frequency data were recorded in analog form on direct-writing, recording-oscillographs

(Visicorder). An additional time reference channel was included on the recorder to improve timing accuracy.

All beams were end mounted in specially fabricated end fixtures that insured positive support and clamping. These beam end-fixtures were inserted into a milling machine type, precision, indexing-chuck that provided both a secure, stable mount and the accurate, repeatable angular settings required for experiments.

Several experiments were made where beam tip-end displacement or static deflection was measured instead of frequency. In these cases, a simple "mapping" on graph paper was made of the beam tip-end elastic axis reference point location as a function of applied load and pitch angle.

Experimental Methods

Various experiments were conducted using the previously described beam specimens and apparatus. The principal parameters varied included blade tip load (P) and blade pitch angle (θ). Figure 2.3 displays the axis system and notation utilized. Figure 2.4 is a schematic showing typical loading procedures and excitation/deflection sense.

In the static deflection experiments, the selected values of pitch angle (measured at the blade root end) were pre-set and locked for each run. A weight bucket was attached to a small machine screw (by a string) at the blade tip elastic axis point. Then, increasing loads using 1/2 pound increments were applied and the beam tip elastic-axis reference point location was "mapped" on graph paper. An example of this data is shown in Figure 2.5.

In the natural frequency experiments, selected tip loads were applied (as shown schematically in Figure 2.4) and the beam natural frequencies were measured as functions of beam pitch angle (measured at the beam root end) and excitation sense. Each tip weight was rigidly attached to the beam tip end and the beam was excited in flapwise as well as chordwise senses, Figure 2.4. Strain gages used as frequency transducers and their associated instrumentation permitted relatively accurate measurement of both the flapwise and chordwise frequencies. All data were collected on direct-writing, recording oscillographs in the form of sinusoidal displacement traces versus time. A typical example of a portion of the data oscillograph is shown in Figure 2.6. Records lengths were of the order of ten to fifteen seconds and because of the additional 60 cycle timing pulse shown on each trace, timing accuracy for the longer record lengths was probably on the order of plus or minus one millisecond. Determination of the peak to peak distances (based on time) for one cycle (or repeated cycles) of flapwise or chordwise motion could be accurately measured to within plus or minus 5 to 15 milliseconds. Considering data record lengths of 5 seconds (5,000 milliseconds) to 15 seconds (15,000 milliseconds), measuring accuracies for frequency using this instrumentation system are on the order of about 1 part in 1,000 or about plus or minus 0.1%.

The determination of flapwise and chordwise frequencies was done in separate experiments. That is, the weight mounted at the tip-end was excited (by hand) in the flapwise sense so that the output trace of fre-

quency in the flapwise sense was of acceptable amplitude whereas, the output trace in the chordwise sense was minimized (or ideally--zero). Then the strain gage trace data were recorded (5 seconds to 15 seconds in length depending on frequency) and the frequency determined from the accurate time trace on the recording chart. The same experiment was then repeated except that the beam was now excited in the chordwise sense with the flapwise motion minimized.

The data measured using this technique and the specified instrumentation are shown in tabular form in Tables I and II.

REPRODUCIBILITY OF THE
ORIGINAL PAGE IS

3. THEORETICAL MODEL

We briefly review the form of the theoretical model and its solution employed here. The basic equations (a Rayleigh-Ritz modal solution) are taken from Hodges[1]. They are generalized to include a tip mass. One modal shape is used for flap, lag and twist and torsional inertia is neglected (Hodges "modified flap-lag equations") on the basis of a large torsional natural frequency compared to flap and lag. The equations are (suitably non-dimensionalized)

$$w_1'' \left[1 + \frac{M_{TIP}}{mR} \psi_1^2 (x/_R = 1\right] + \beta_1^4 w_1 - K_{111}^2 \frac{(e-1)^2 v_1^2 w_1}{g\gamma_1^2}$$

$$= \left[\frac{mgR^3}{EI_{y'}} \int_0^R \dot{\psi}_1 \frac{dx}{R} + \frac{M_{TIP} g}{EI_{y'}} R^2 \psi_1 (x/_R = 1)\right] \sin\theta \qquad (1)$$

$$v_1'' \left[1 + \frac{M_{TIP}}{mR} \psi_1^2 (x/_R = 1)\right] + e\, \beta_1^4 v_1 - K_{111}^2 v_1 w_1^2 \frac{(e-1)^2}{g\gamma_1^2}$$

$$= \left[\frac{mgR^3}{EI_{y'}} \int_0^R \psi_1 \frac{dx}{R} + \frac{M_{TIP} g R^2}{EI_{y'}} \psi_1 (x/_R = 1)\right] \cos\theta$$

In the above, the following twist equation of equilibrium was used to eliminate the twist angle, i.e.

$$g\gamma_1^2\,\phi_1 + K_{111}\,v_1 w_1\,(e-1) = 0 \qquad (2)$$

The various coefficients are given by

$$e = \frac{EI_{z'}}{EI_{y'}}$$

$$g = \frac{GJ}{EI_{y'}}$$

$$K_{111} = 5.039$$

$$\gamma_1 = \pi/2$$

$$\beta_1 = 1.875$$

Also

ψ_1 - natural bending mode of a non-rotating, uniform cantilever normalized so that

$$\psi_1(x/_p = 1) = 2$$

v_1, w_1, ϕ_1 - generalized coordinates of lag, flap and twist respectively

$$'' \equiv \left(\frac{d^2}{dt^2}\right)\frac{mR^4}{EI_{y'}}$$

For our purpose v_1, w_1 may be expressed as the sum of static and dynamic equlibrium values, i.e.

$$v_1 = v_1^{o} + \hat{v}_1 \ (t)$$
$$w_1 = w_1^{o} + \hat{w}_1 \ (t) \qquad (3)$$

where v_1^{o}, w_1^{o} are, by definition, independent of time. Substituting (3) into (1) we may obtain (nonlinear) equations for v_1^{o}, w_1^{o} by deleting the time derivatives in (1). The (linear) perturbation equations for $\hat{v}_1$, $\hat{w}_1$ are obtained in the usual way from (3) and (1) by assuming they are small (compared to v_1^{o}, w_1^{o}), namely

$$\hat{w}_1'' \ \mu_o + \beta_1^4 \ \hat{w}_1 - D \ [v_1^{o2} \ \hat{w}_1 + 2 \ w_1^{o} \ v_1^{o} \ \hat{v}_1] = 0$$

$$\hat{v}_1'' \ \mu_o + e\beta_1^4 \ \hat{v}_1 - D \ [w_1^{o2} \hat{v}_1 + 2 \ w_1^{o} \ v_1^{o} \ \hat{w}_1] = 0 \qquad (4)$$

where $\mu_o \equiv 1 + \dfrac{M_{TIP}}{mR} \ \psi_1^2 \ (x/_R = 1)$

$$D \equiv \left(\frac{K_{111}}{\gamma_1}\right)^2 \frac{(e-1)^2}{g}$$

From (4), having first computed the static solutions, we may calculate the flap, lag natural frequencies.

In particular, for $e > 1$ and $\theta = 0^{o}$, we may compute the lateral buckling load as follows. For $\theta = 0^{o}$, we see that

$$w_1^{o} = 0$$

$$v_1^{o} = \frac{\left[\dfrac{mgR^3}{EI_{y'}} \displaystyle\int_0^R \psi_1 \frac{dx}{R} + \frac{M_{TIP}}{EI_{y'}} \ gR^2\psi_1(x/_R = 1)\right]}{e \ \beta_1^4} \qquad (5)$$

The lateral buckling condition may be identified as the vanishing of the flap frequency. From (4) this means

$$\beta_1^4 - D\, v_1^{o2} = 0 \tag{6}$$

From (5) and (6), we may determine the tip weight at which buckling occurs as (neglecting weight of beam which is generally small compared to tip weight)

$$M_{TIP}\, g \approx 6.8 \sqrt{\frac{EI_{y'}\, GJ}{R^2}} \left(\frac{e}{e-1}\right) \tag{7}$$

Timoshenko's exact analysis[3] of this problem (effectively an infinite number of modal shapes were used) gives (7) with the numerical factor 6.8 replaced by 4.013. (Also it should be noted that Timoshenko assumed $e >> 1$ and hence $e/(e-1) \approx 1$. The above formula does not have this restriction). Using this result one might empirically modify the single mode analysis by adjusting D so that one obtains the Timoshenko numerical factor. It should be emphasized that the Timoshenko and Hodges-Dowell theories for lateral buckling are essentially identical. It is only in the use of a single mode solution procedure that we have been led to a different numerical factor.

4. EXPERIMENTAL RESULTS AND COMPARISON WITH THEORY

Static Deflections:

Results have been obtained for two beams, one of 1/2" x 1/8" cross-section, the other of 1" x 1/8", and both 20" in length. The static experimental loading is a simple weight (denoted by P, see Figure 4.1) with the beam rotated to achieve various loading angles. Measurements of flap and lag bending deflection at the beam tip, W_{TIP} and V_{TIP}, have been obtained for $\theta = 0^{\circ} \rightarrow 90^{\circ}$ and for $P = 0 \rightarrow 5^{\#}$. Representative results are presented in Figure 4.2 - 4.7.

As predicted by theory, there are no significant nonlinearities for $\theta = 0^{\circ}$ and 90°. See Figure 4.2. For intermediate angles, e.g. 30° in Figure 4.3 and 4.6, nonlinear behavior is clearly evident. The correlation between theory and experiment is generally satisfactory for the linear regime and also for the initial deviation from linear behavior into the nonlinear regime. However, when one of the deflection components (usually W_{TIP}) becomes a substantial fraction of beam radius, the theory (which assumes $\frac{W_{TIP}}{R}$, $\frac{V_{TIP}}{R}$ much less than 1) is inadequate. Indeed theory predicts a reversal and/or jump in the load deflection curve (see Figure 4.4A and 4.4B) but such behavior has not been observed experimentally.

It would be very desirable to measure the twist of the beam as well. Theory predicts that its variation with load is nonlinear even for very small loads.

Natural Frequencies:

Results have been obtained for two beams, one 20" long and the other 30", and both of cross-section 1/2" x 1/8". Measurements of flap and lag frequencies have been obtained for $\theta = 0^{\circ} \rightarrow 90^{\circ}$ and P up to $10^{\#}$ for $\theta = 0^{\circ}$. A rather complete set of results is presented in Figure 4.8 - 4.17. In Figure 4.8 experimental results are shown for $P = 1,2,3,4^{\#}$ over a range of θ. Nonlinear theoretical results for the same conditions are shown in Figure 4.9. Linear theory would predict no change in frequency with θ (the lag results being those for $\theta = 0^{\circ}$ and the flap results those for $\theta = 90^{\circ}$). As can be seen the trends of the theoretical and experimental data are similar. As expected, both theory and experiment show a convergence of frequencies as $\theta \rightarrow 90^{\circ}$. The dead weight load has (theoretically) no effect on the flapwise mode for $\theta = 90^{\circ}$ or the chordwise mode for $\theta = 0^{\circ}$. The weight still contributes a dynamic mass effect, of course.

A more detailed comparison of experimental and theoretical results is shown in Figure 4.10 - 4.15. The correlation between theory and experiment is much better for the chordwise than the flapwise mode. Systematic deviations for the latter occur for increasing angle and/or tip weight.

As noted above, there is a systematic discrepancy between (nonlinear) theory and experiment for flapwise natural frequencies as a function of increasing static loading. It was hypothesized that this might be due to the finite dimensions of the tip weights, particularly for the larger tip weights used in the experiment. Thus, a longer beam (30" vs 20") was

tested. This beam also requires smaller tip weights; hence the dimensions of the tip weights compared to beam length were much smaller then for the 20" beam. The results for both the 20" and 30" beams with $\theta = 0^{\circ}$ are shown in Figure 4.16 and 4.17. The systematic discrepancy remains. It now seems plausible that this is a defect in the solution to the theoretical model. In particular it may be a result of using only a single mode in the Rayleigh-Ritz procedure which is inaccurate for large tip weights.

To test this latter hypothesis we have shown two additional theoretical results in Figure 4.16, namely those from linear theory and those from nonlinear theory with an empirical correction to give the known theoretical buckling load[3]. The buckling load is that value of P for which the flap frequency goes to zero. As may be seen, linear theory is in poor agreement with the experimental data for large tip weights and, in particular, does not predict any buckling at all. In the linear model the decrease in flap frequency is solely due to the mass of the tip weight. The nonlinear theory (without any empirical correction) is in better agreement with the experimental data and predicts buckling at a load approximately 50% higher than that measured. The nonlinear theory (with empirical correction to give the known theoretical buckling load) is in much better agreement with the experimental data.

Similar results are shown in Figure 4.17 for the chordwise frequency; there is no difference, for the range of parameters shown, among the linear and the two forms of nonlinear theories.

Clearly, it is desirable to use a larger number of modes in the solution procedure, since we are assured the results will converge to the

known buckling load[3]. Also it would be very desireable to measure the static and dynamic shapes of the beam for various θ and P to verify the above assessment of the reason for the present differences between theory and experiment.

5. CONCLUSIONS AND RECOMMENDATIONS

From the correlation of theory and experiment, we see there is qualitative agreement. The solutions to the theoretical model used a single mode shape in flap and lag. By making an empirical correction to the single mode theoretical model so that the known lateral buckling load (static load in lag direction for which flap frequency is zero) is given, one obtains improved agreement between theory and experiment. This suggests that by including a larger number of modes in the theoretical model so as to obtain the known lateral buckling load, a systematic improved correlation with the experimental data may be obtained. Clearly this should be done to establish more firmly the basic accuracy of the theoretical model. Also measurements of distribution of beam bending and twist and their variation with the magnitude and direction of loading should be made. This will allow a firmer evaluation of the theoretical model and a better understanding of any remaining differences between theory and experiment.

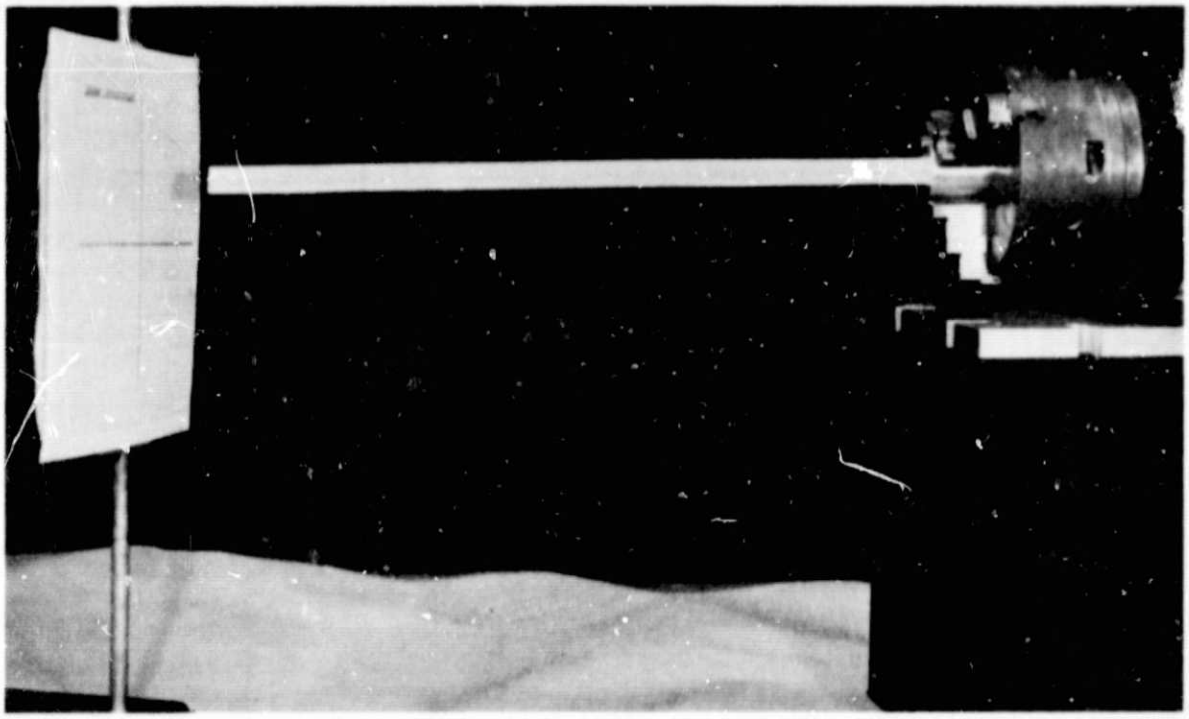

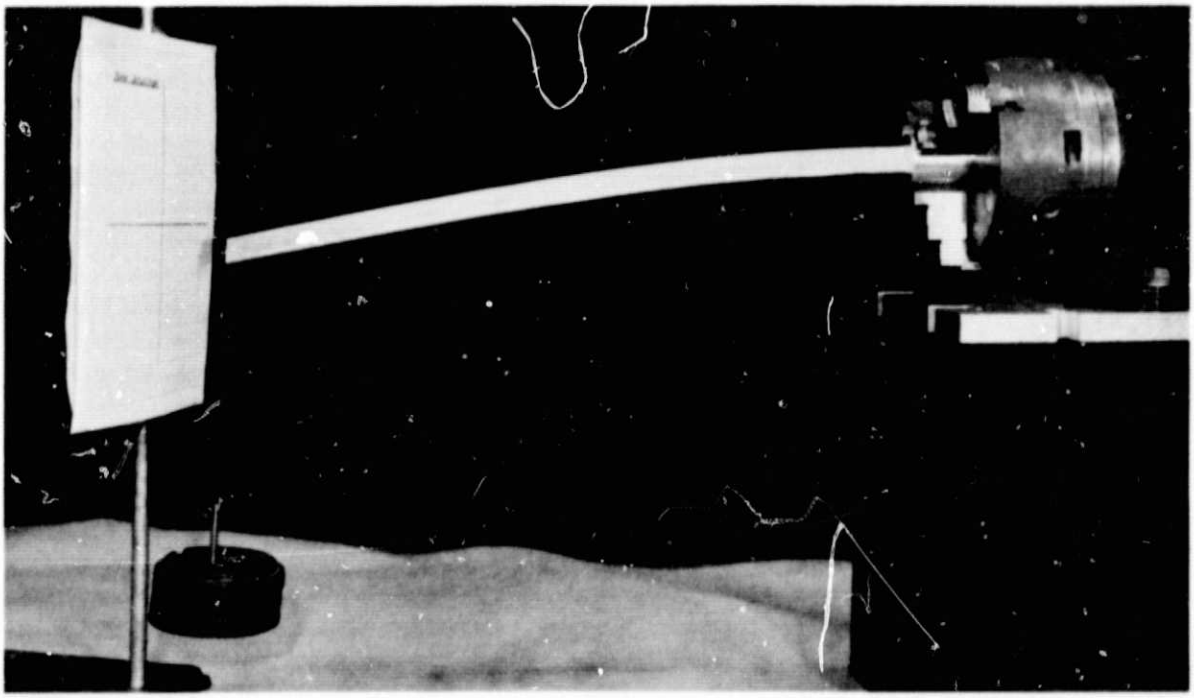

Figure 2.1. Photograph of Apparatus and Set-up for Static Deflection Experiments Showing Loaded and Unloaded Conditions.

REPRODUCIBILITY OF THE
ORIGINAL PAGE IS POOR

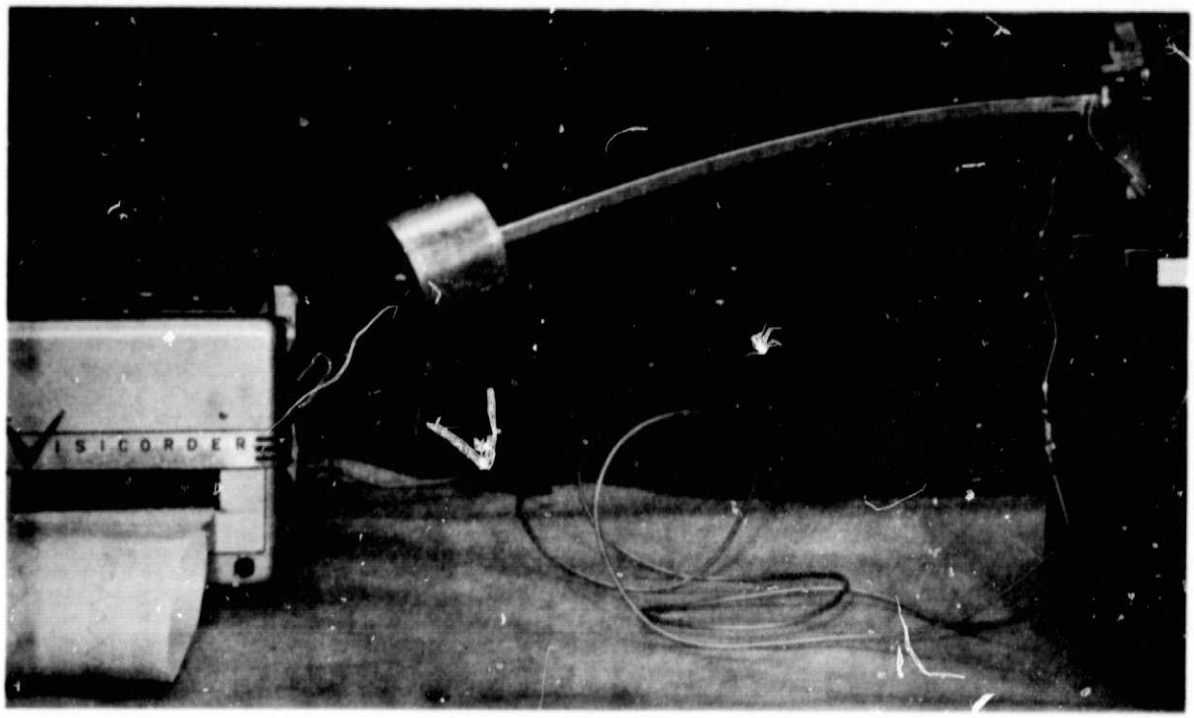

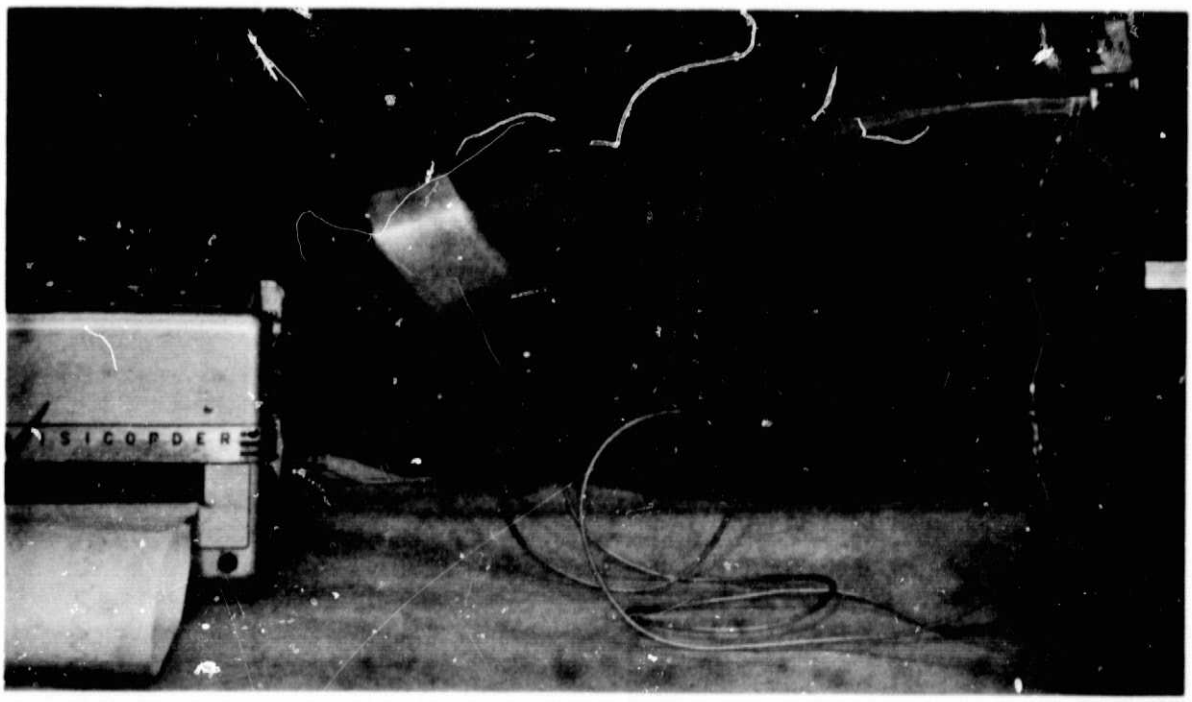

Figure 2.2. Photograph of Apparatus and Set-up for Frequency Measurement Experiments Showing Steady and Oscillating Conditions.

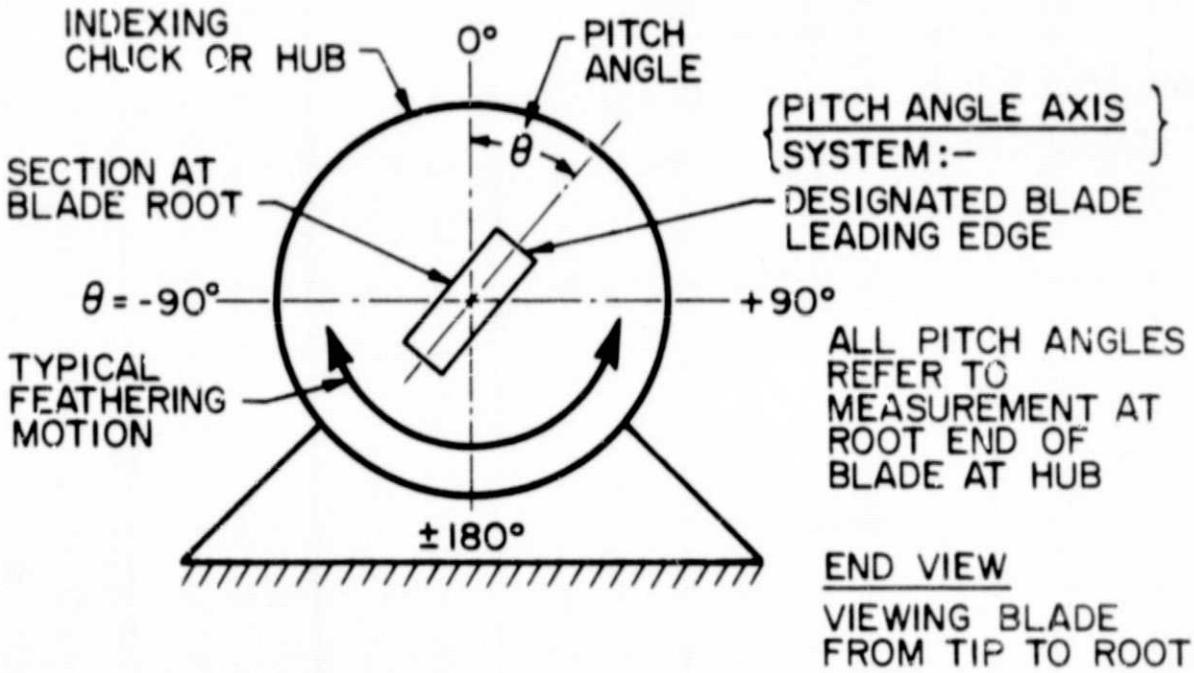

FIGURE 2.3· AXIS SYSTEM AND NOTATION

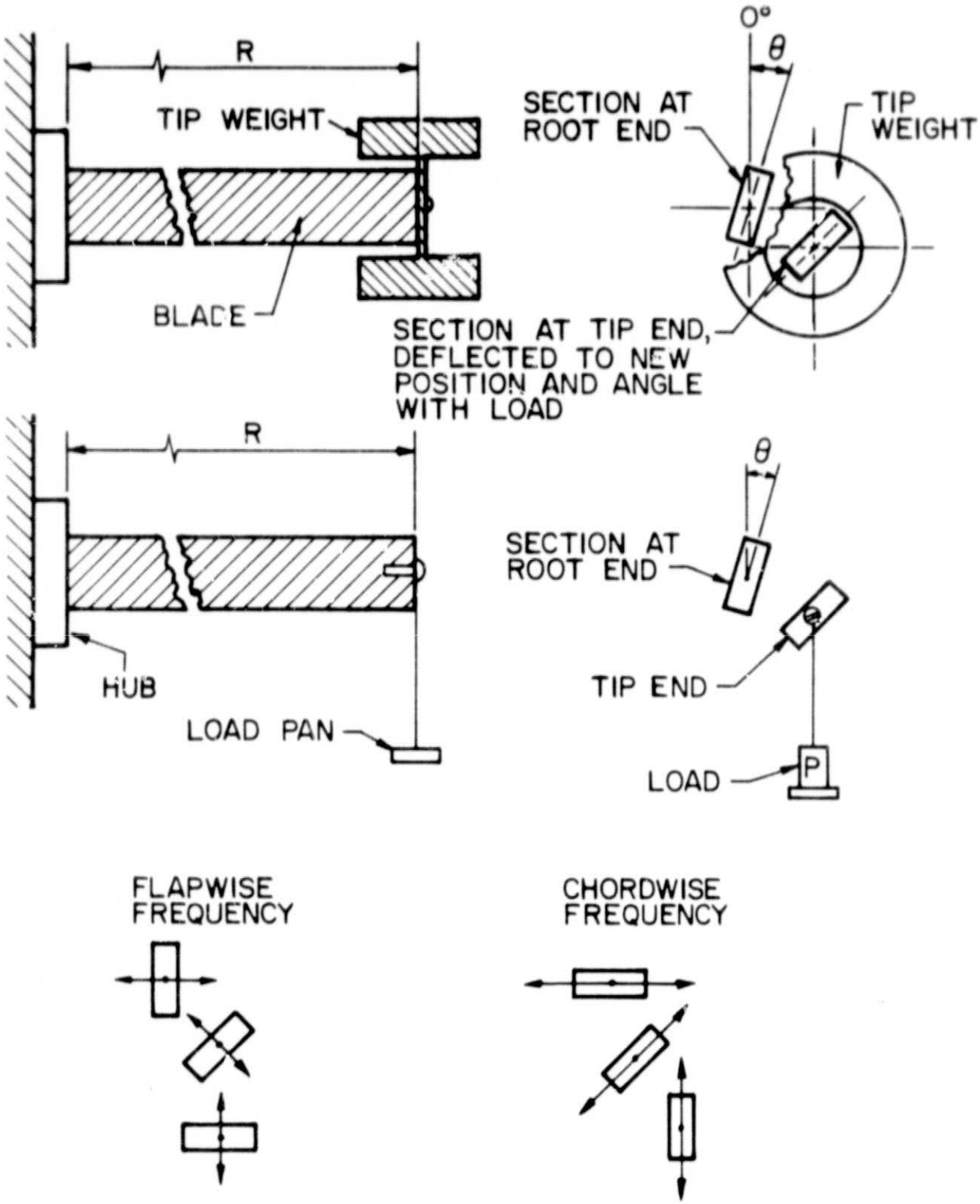

FIGURE 2.4 · SCHEMATIC SHOWING TYPICAL LOADING PROCEDURES AND EXCITATION/DEFLECTION SENSE

REPRODUCIBILITY OF THE ORIGINAL PAGE IS POOR

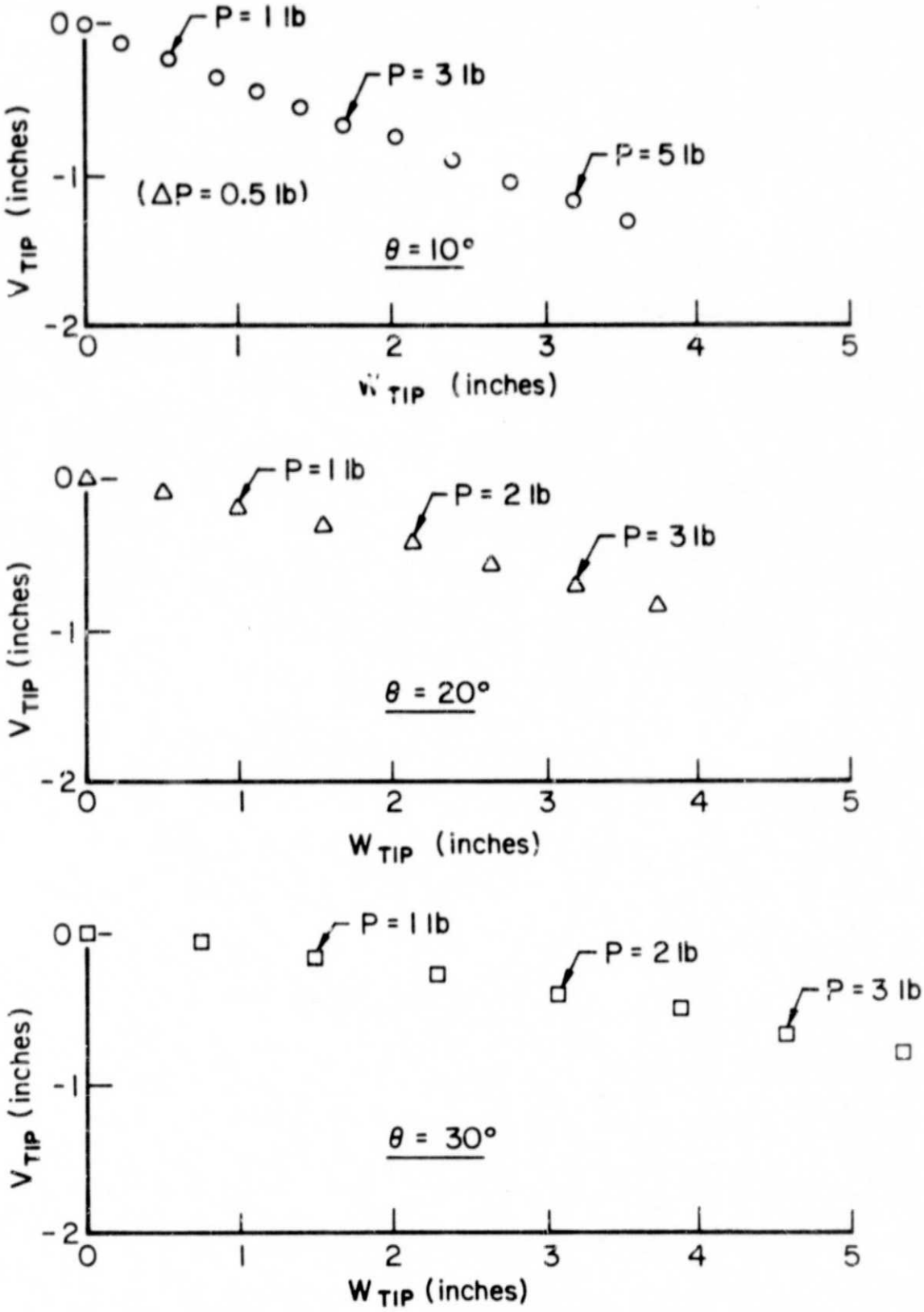

FIGURE 2.5 · STATIC DEFLECTION OF BLADE TIP ELASTIC-AXIS REFERENCE POINT WITH APPLIED LOAD FOR SEVERAL PITCH ANGLES

REPRODUCIBILITY OF THE
ORIGINAL PAGE IS POOR

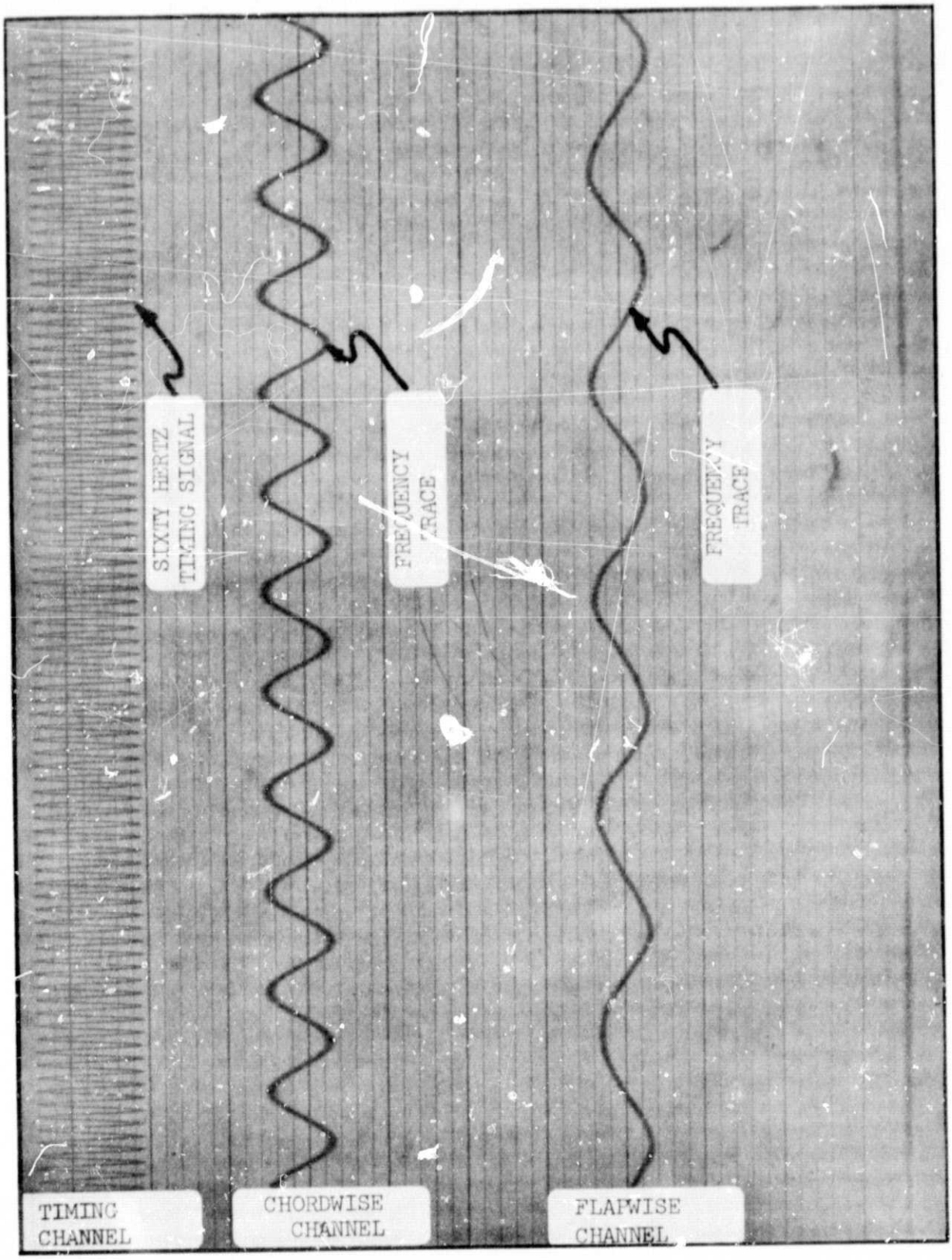

Figure 2.6. Typical Segment of Recording-Oscillograph Chart for Frequency Data.

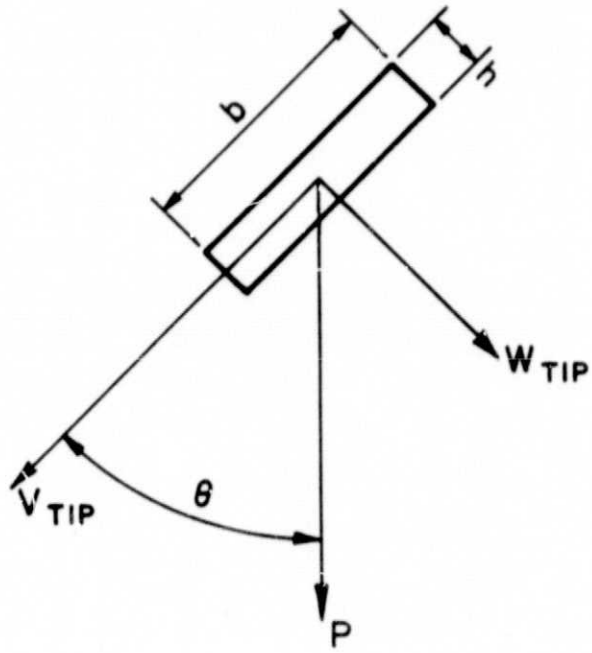

FIGURE 4.1 - GEOMETRY

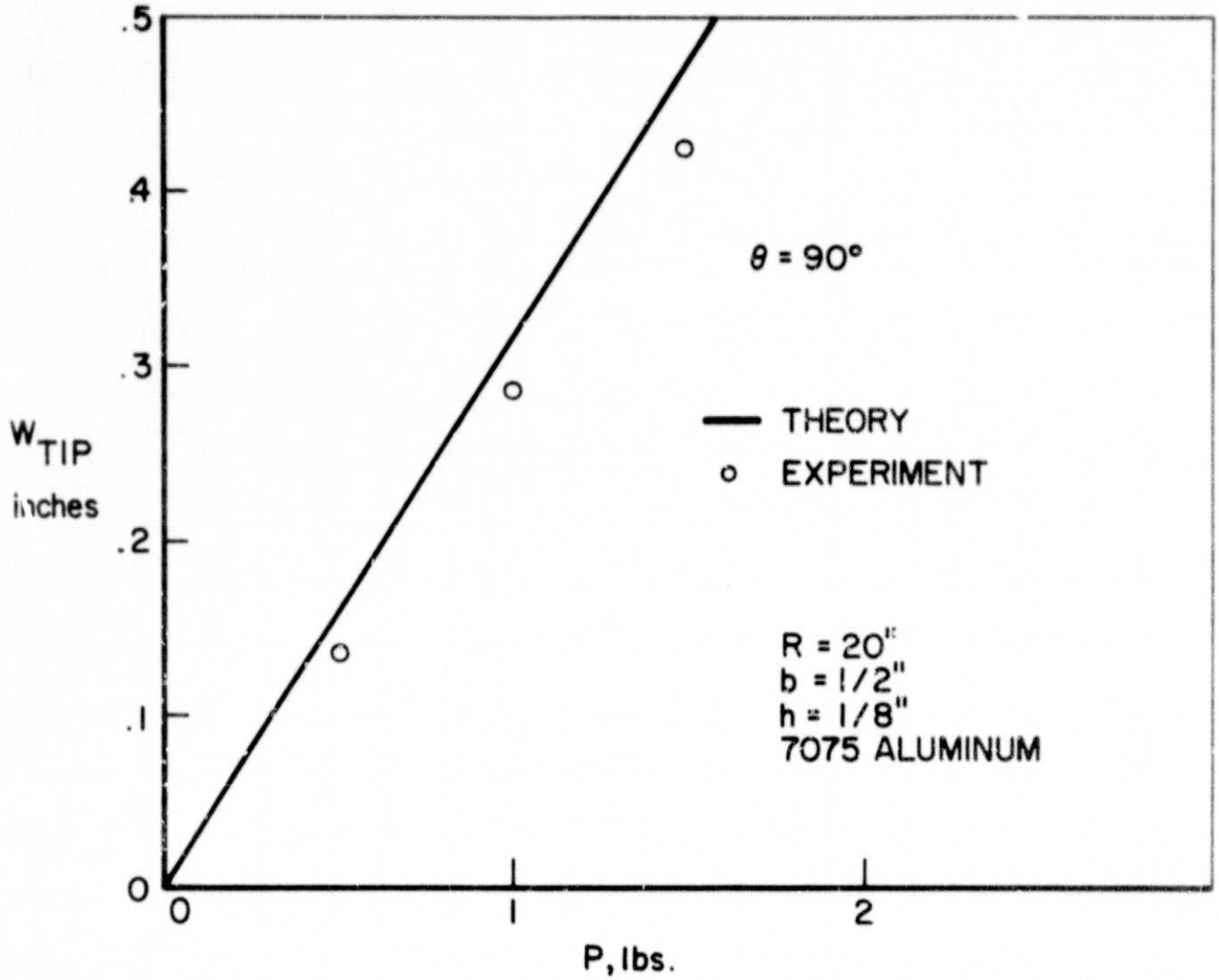

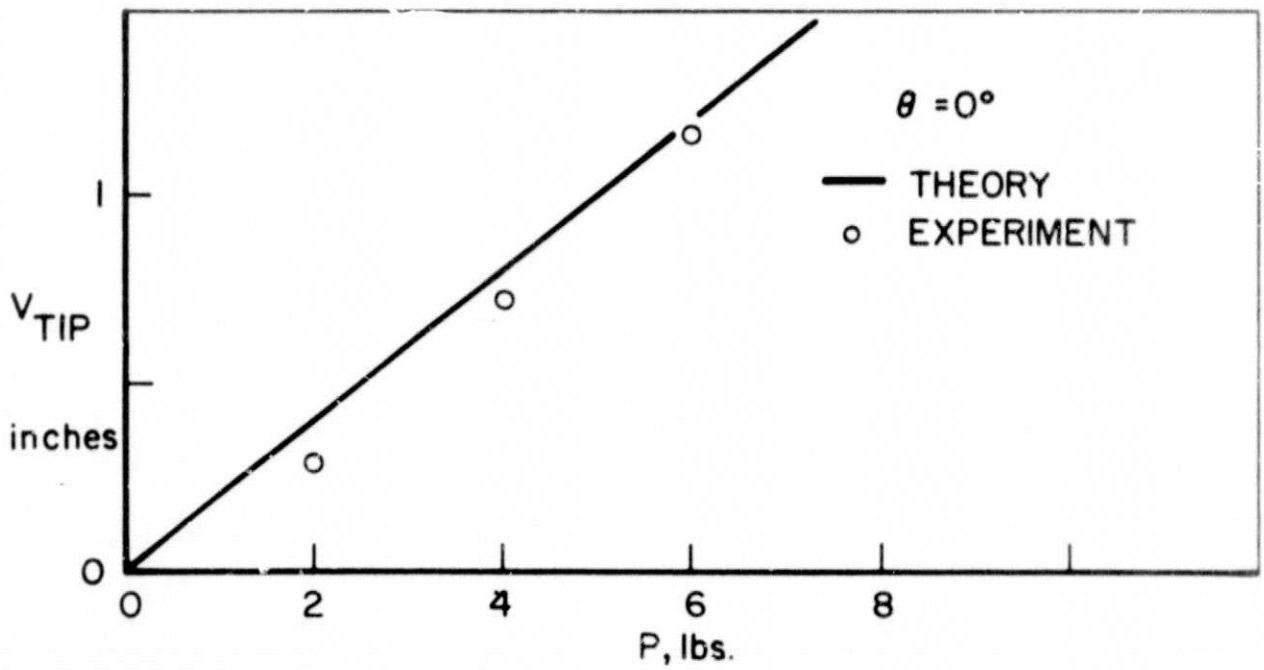

FIGURE 4.2 DEFLECTION VS LOAD

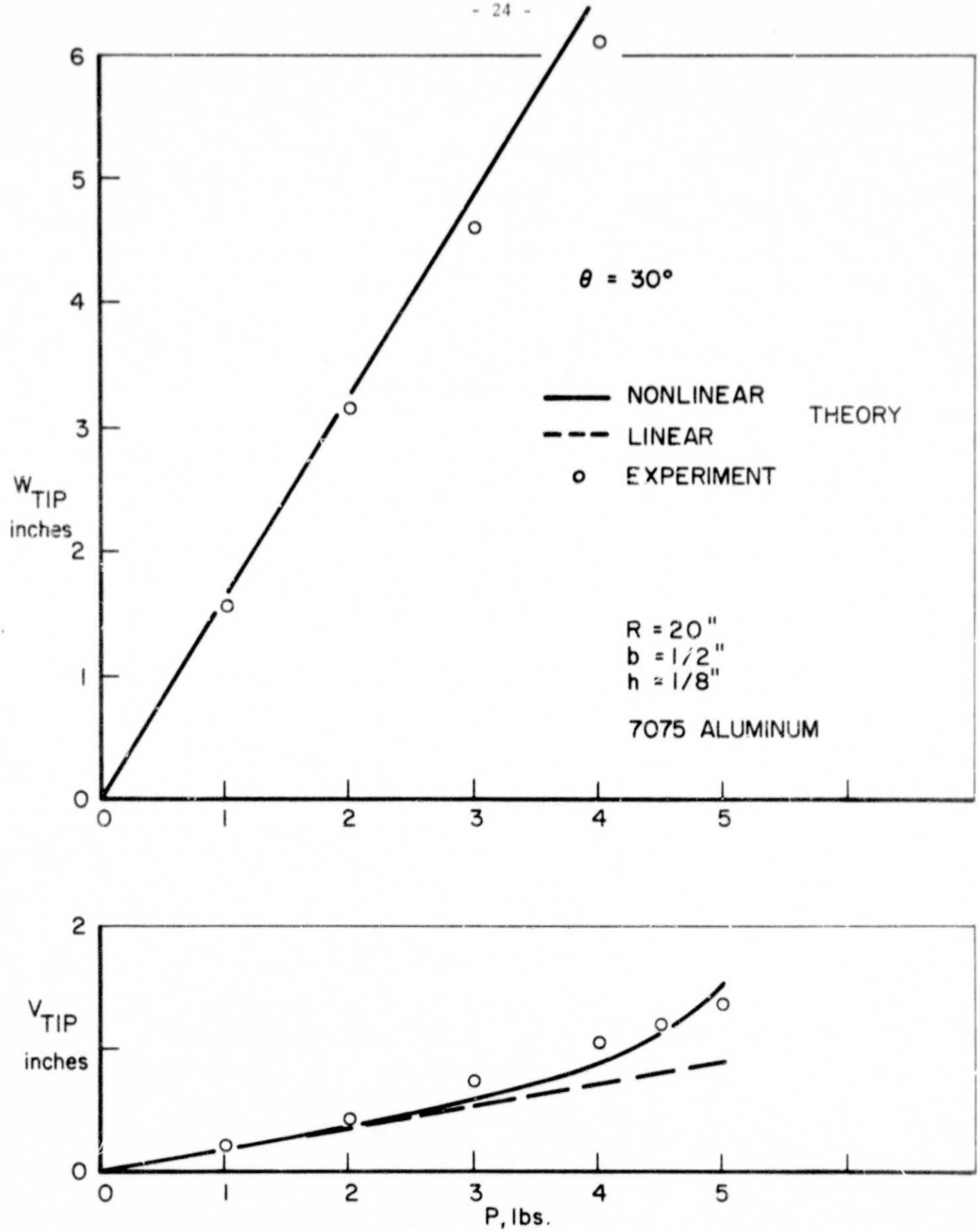

FIGURE 4.3 DEFLECTION VS LOAD

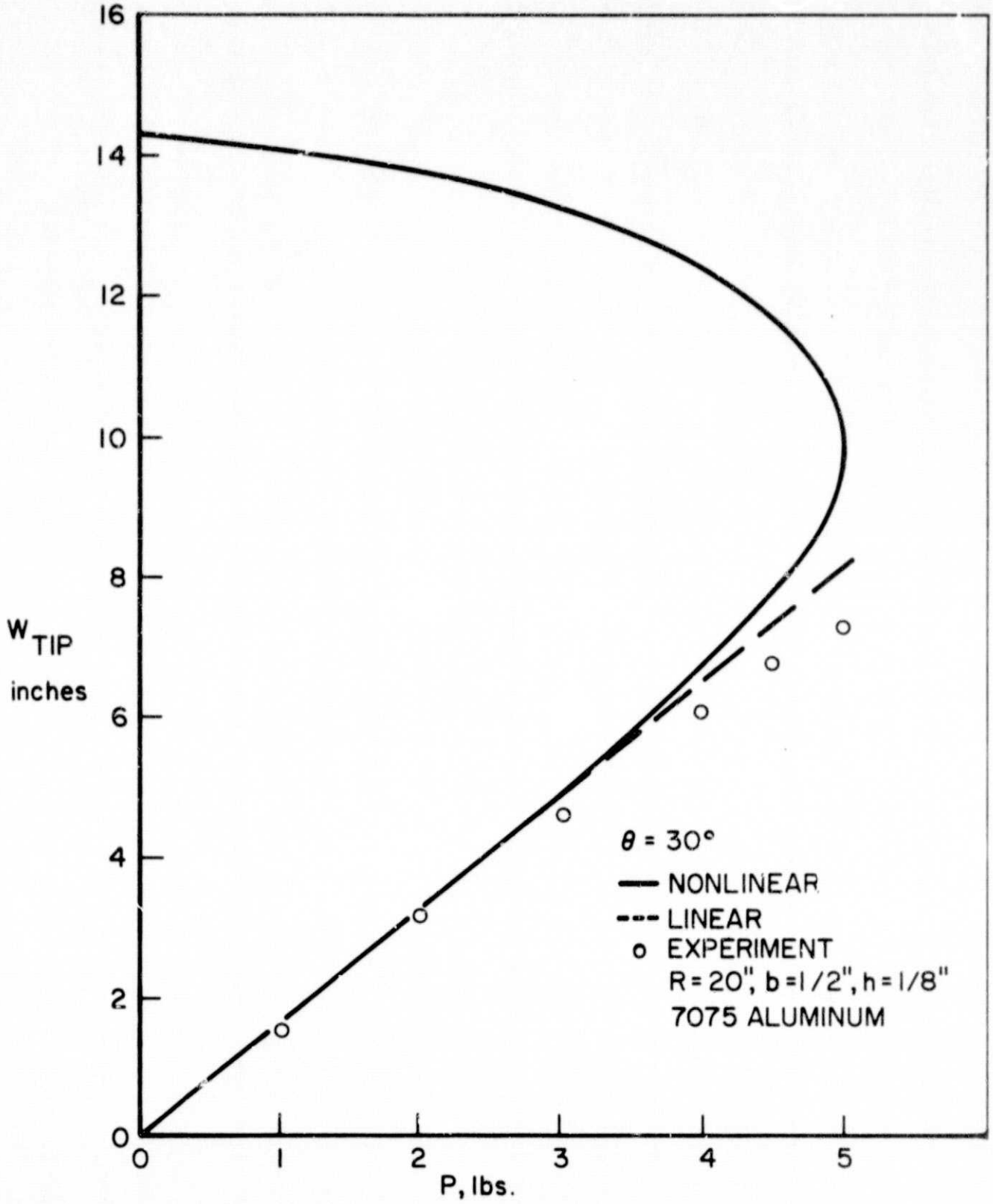

FIGURE 4.4A DEFLECTION VS LOAD

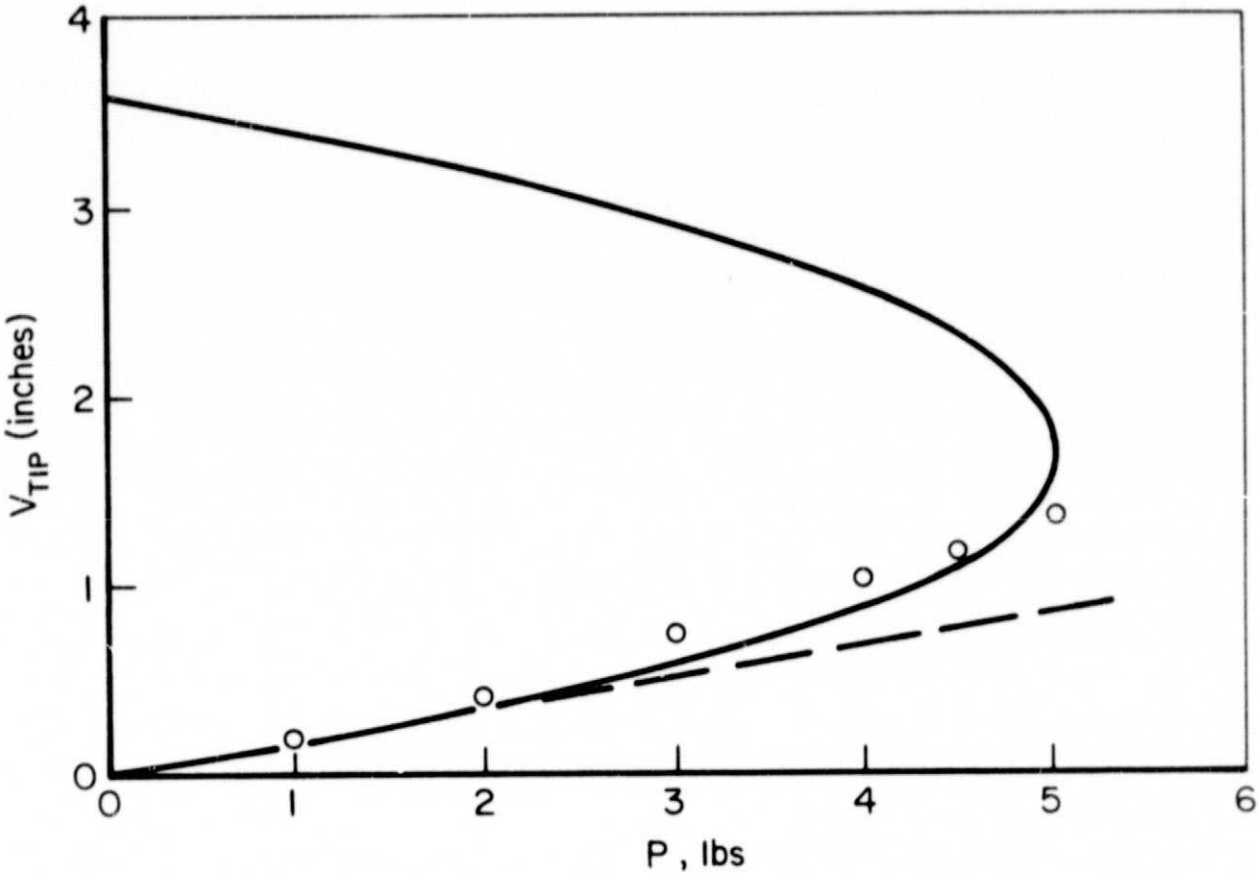

FIGURE 4.4 B · DEFLECTION vs LOAD

REPRODUCIBILITY OF THE ORIGINAL PAGE IS POOR

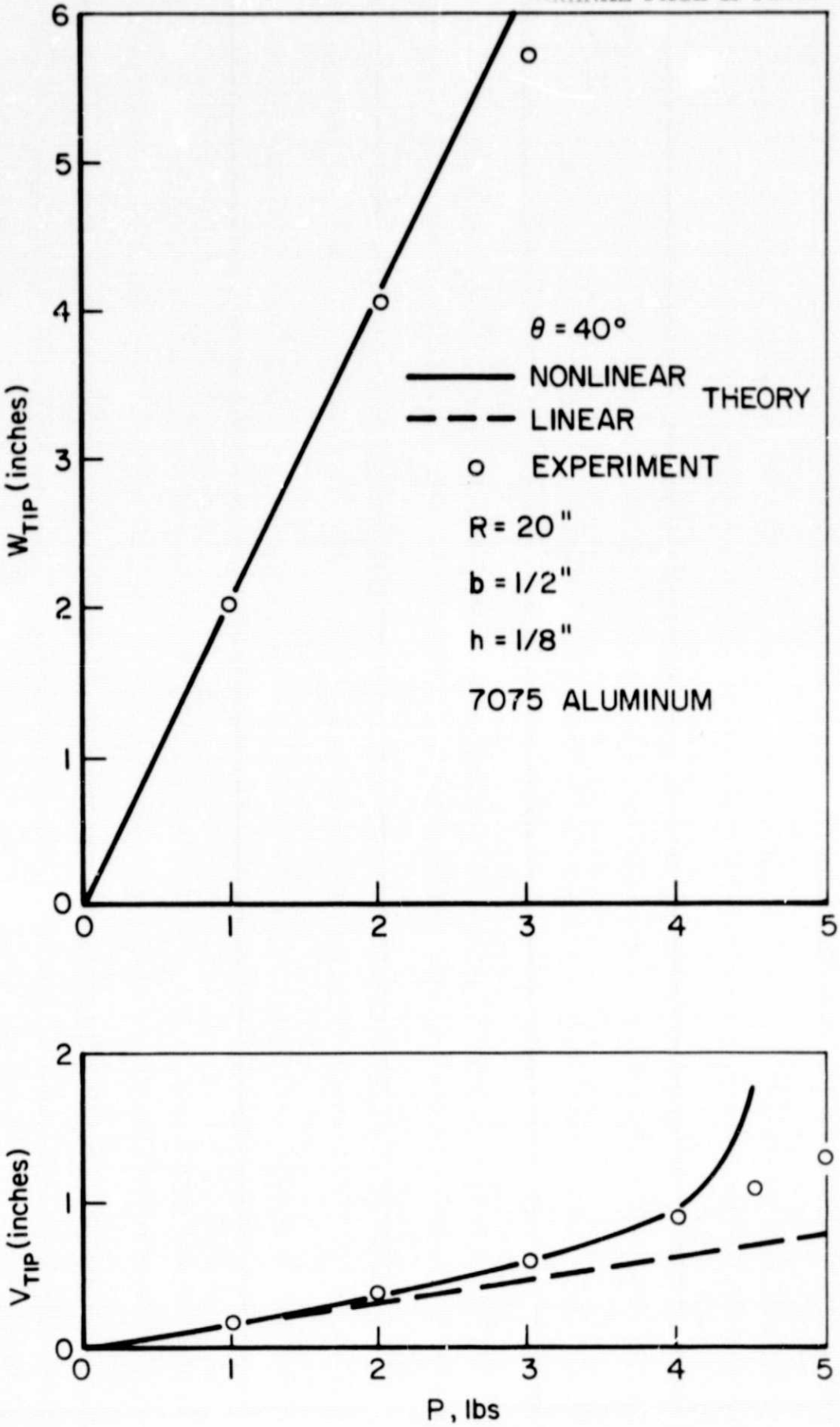

FIGURE 4.5 · DEFLECTION vs LOAD

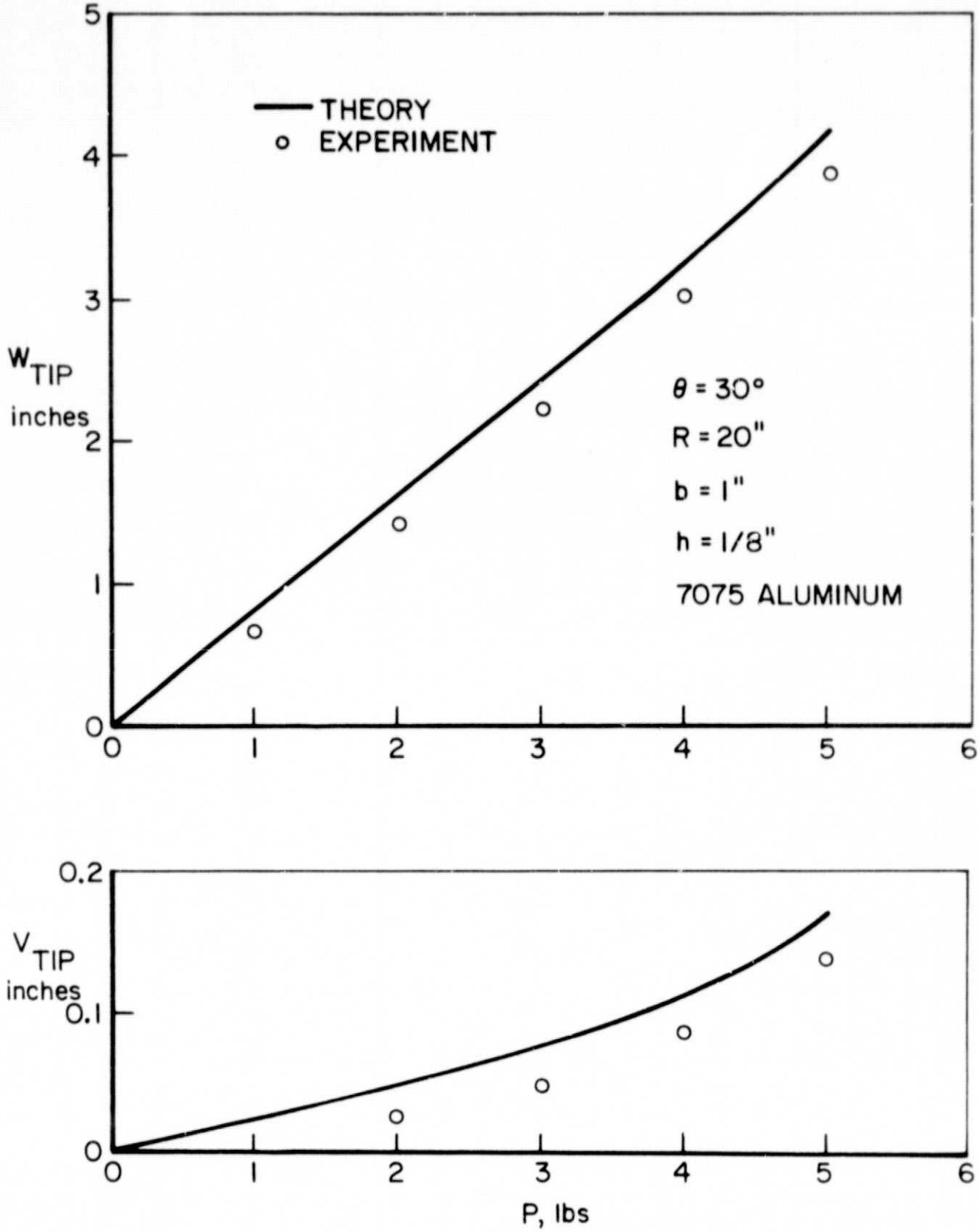

FIGURE 4.6 · DEFLECTION vs LOAD

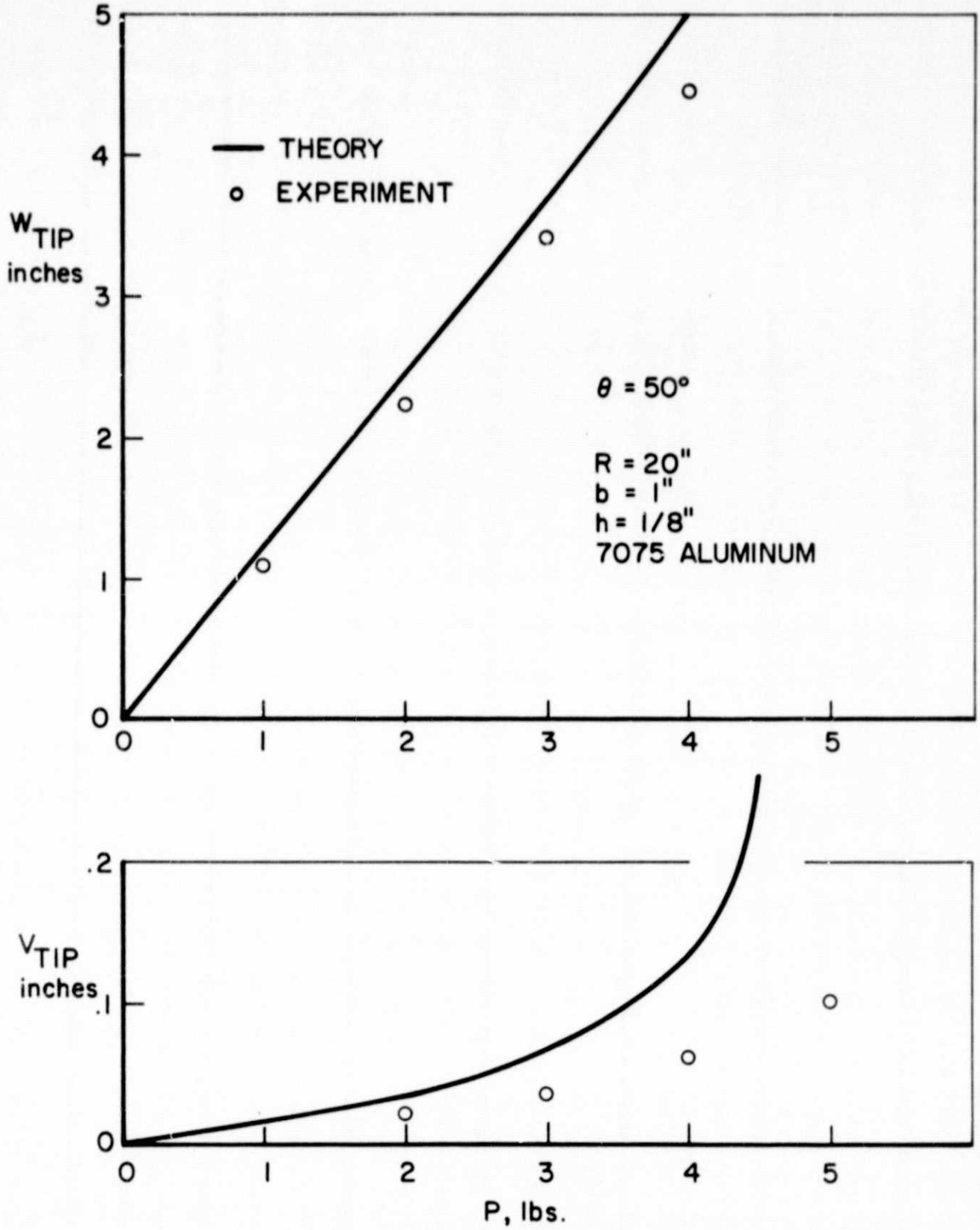

FIGURE 4.7 · DEFLECTION vs LOAD

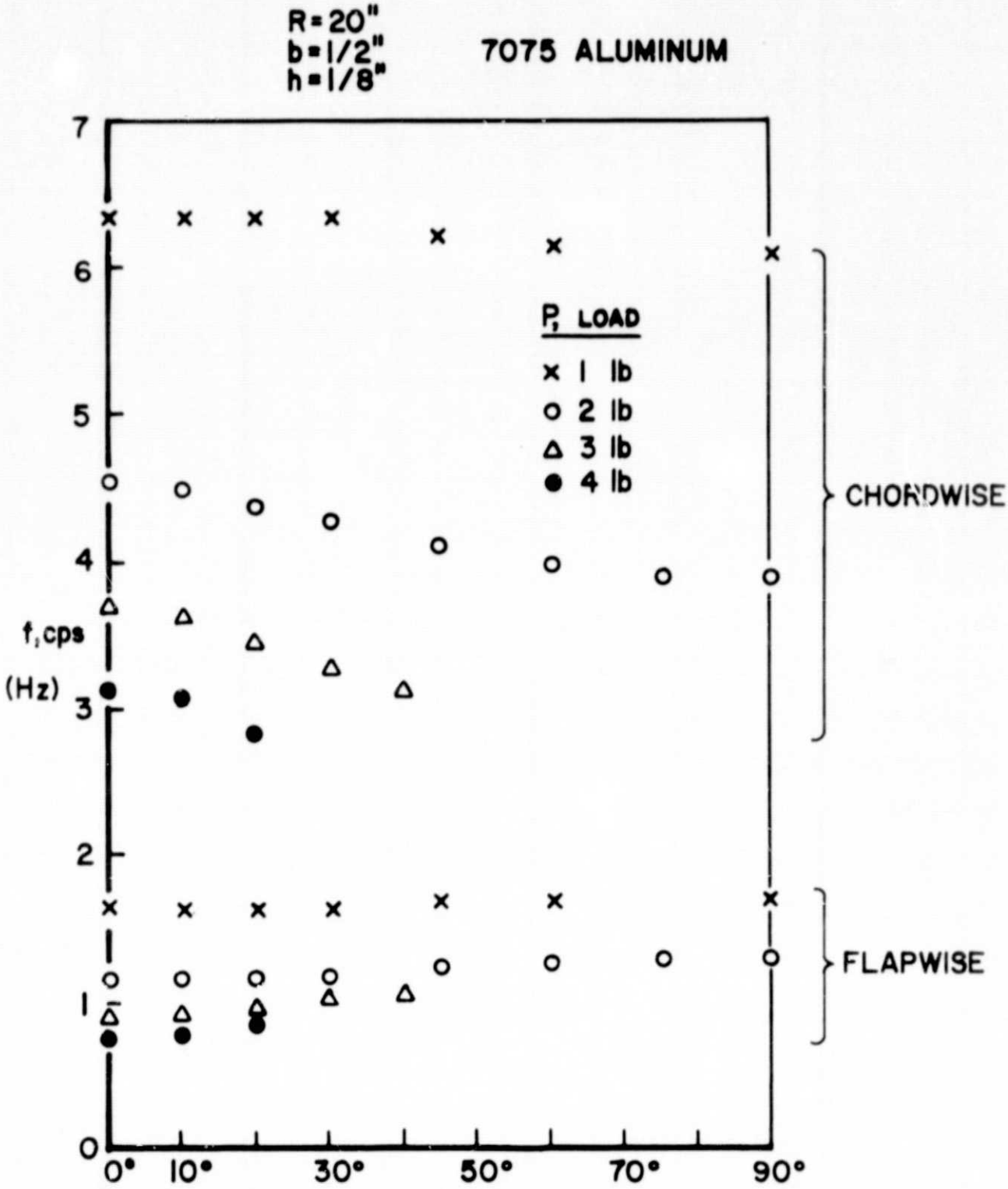

FIGURE 4.8 - NATURAL FREQUENCY VS DEAD WEIGHT LOADING ORIENTATION - EXPERIMENTAL

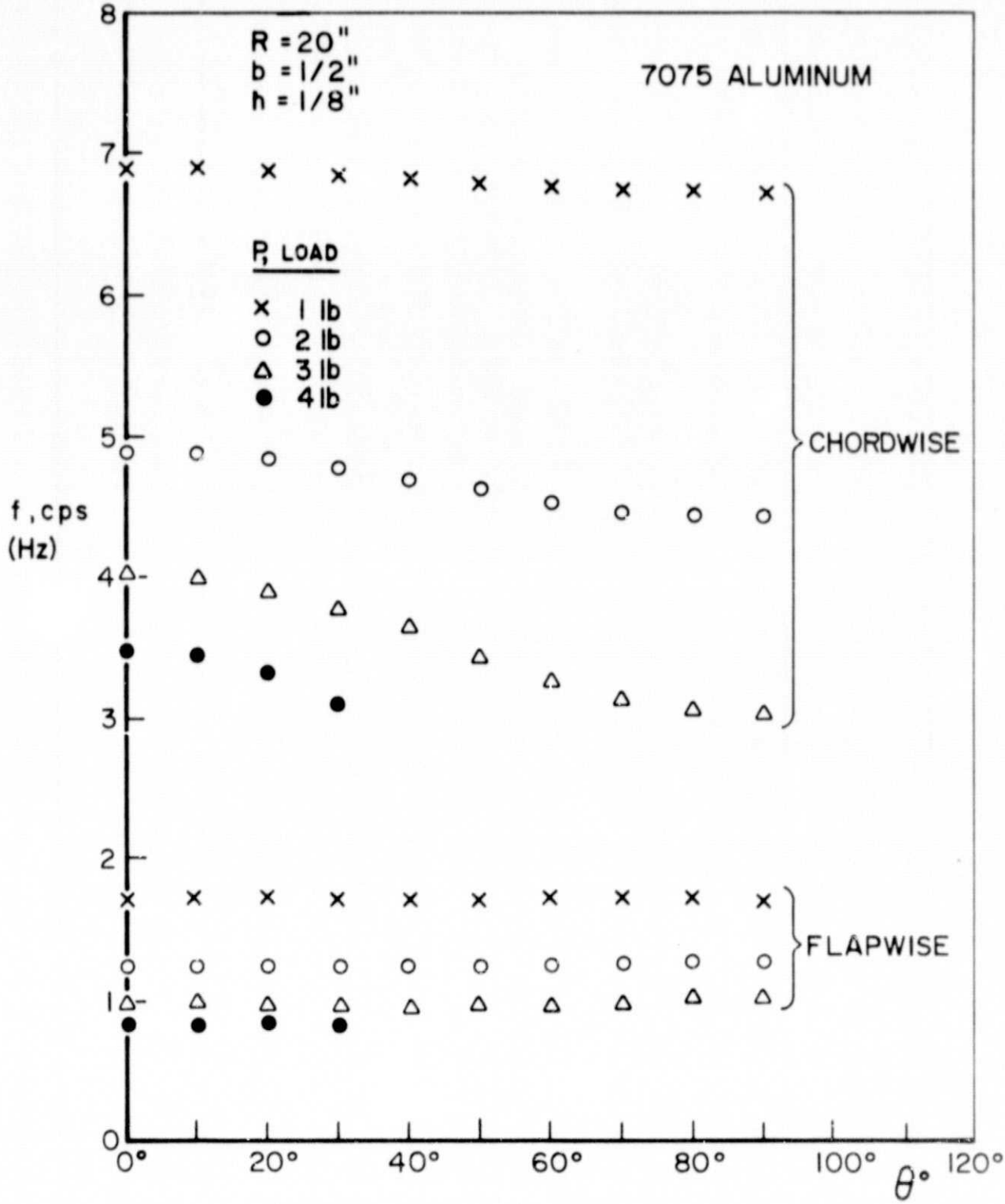

FIGURE 4.9 · NATURAL FREQUENCIES vs DEAD WEIGHT LOADING ORIENTATION THEORETICAL, FF = 1.0

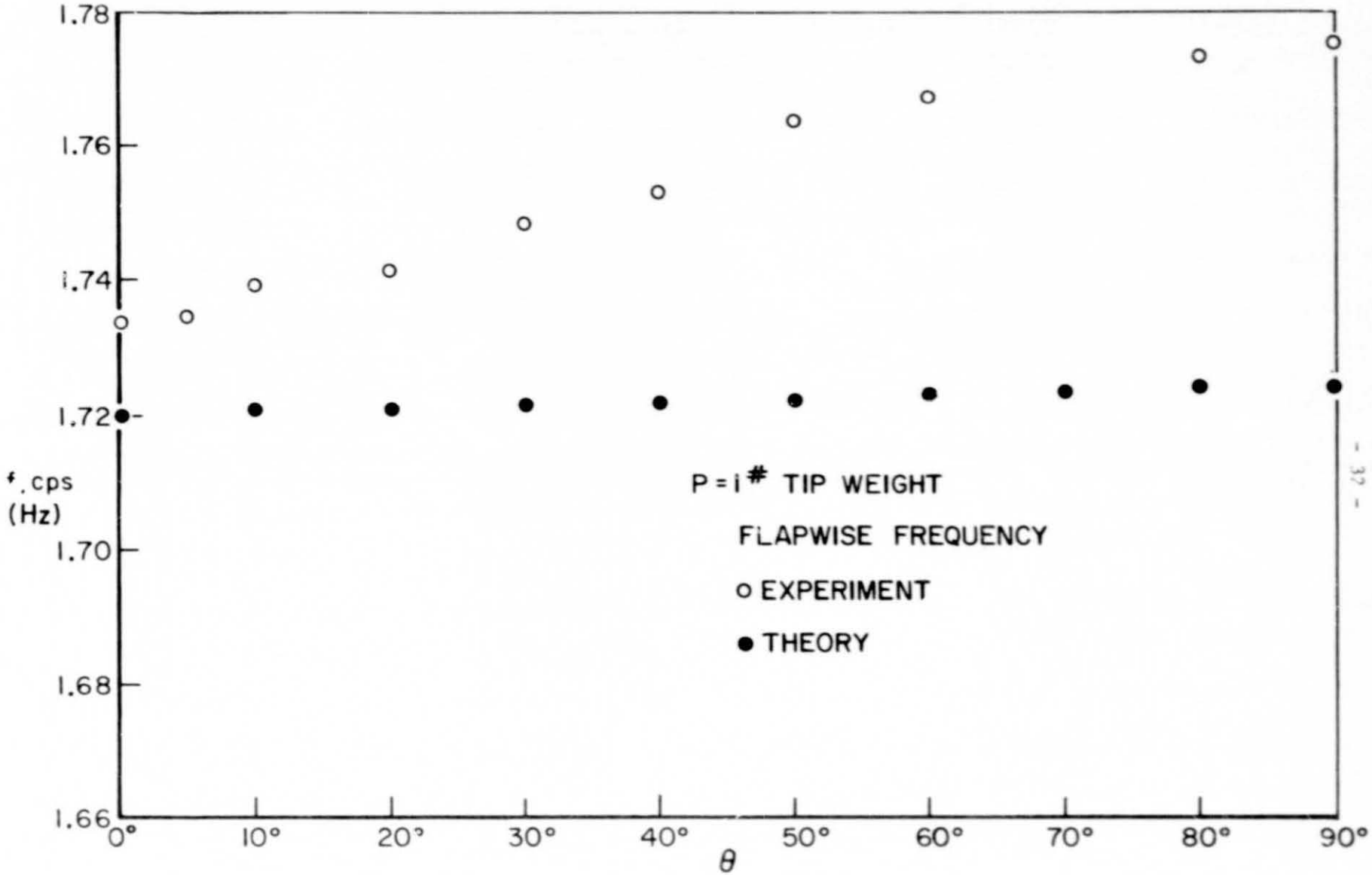

FIGURE 4.10 · NATURAL FREQUENCIES vs PITCH ANGLE

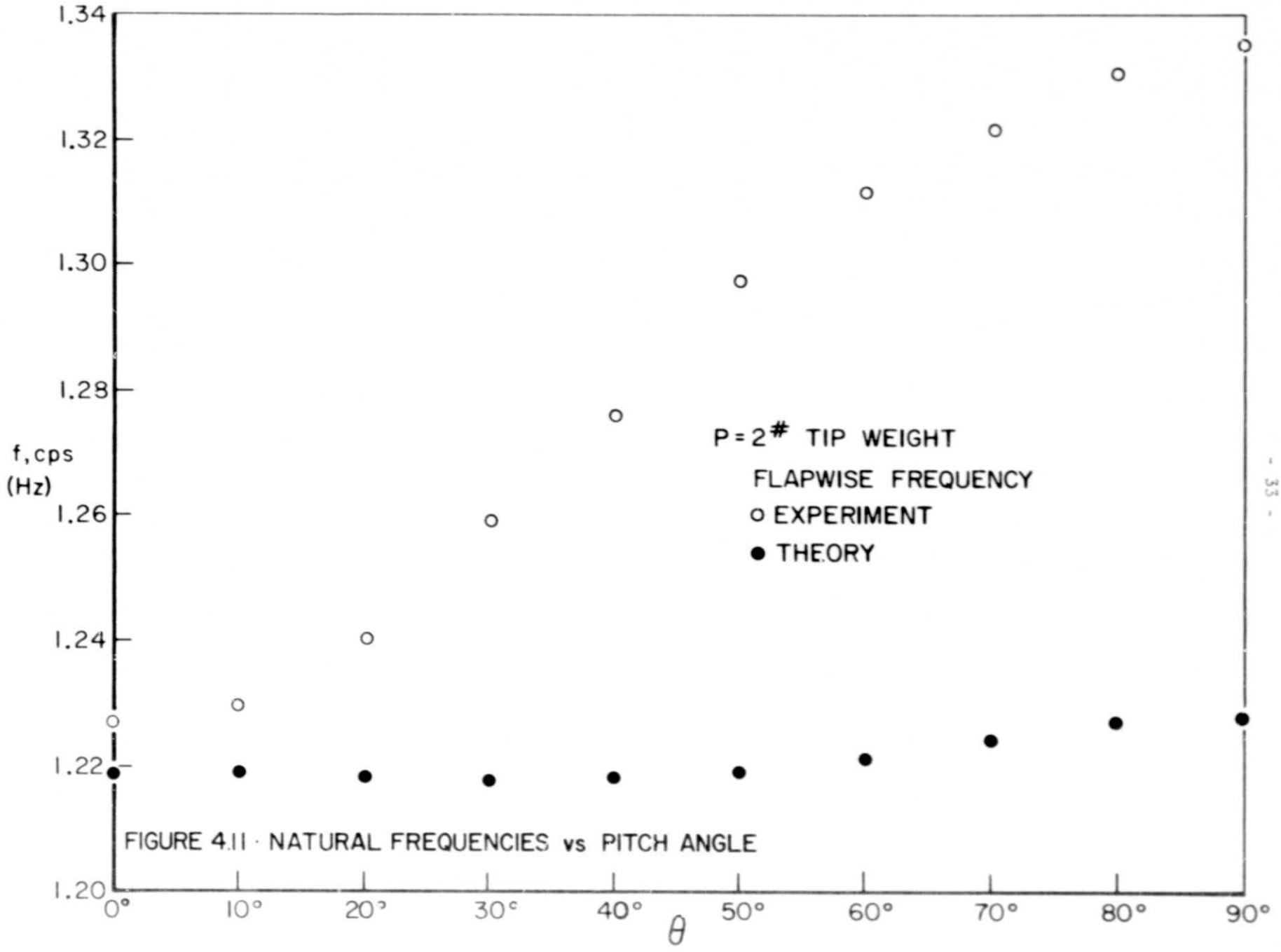

FIGURE 4.11 · NATURAL FREQUENCIES vs PITCH ANGLE

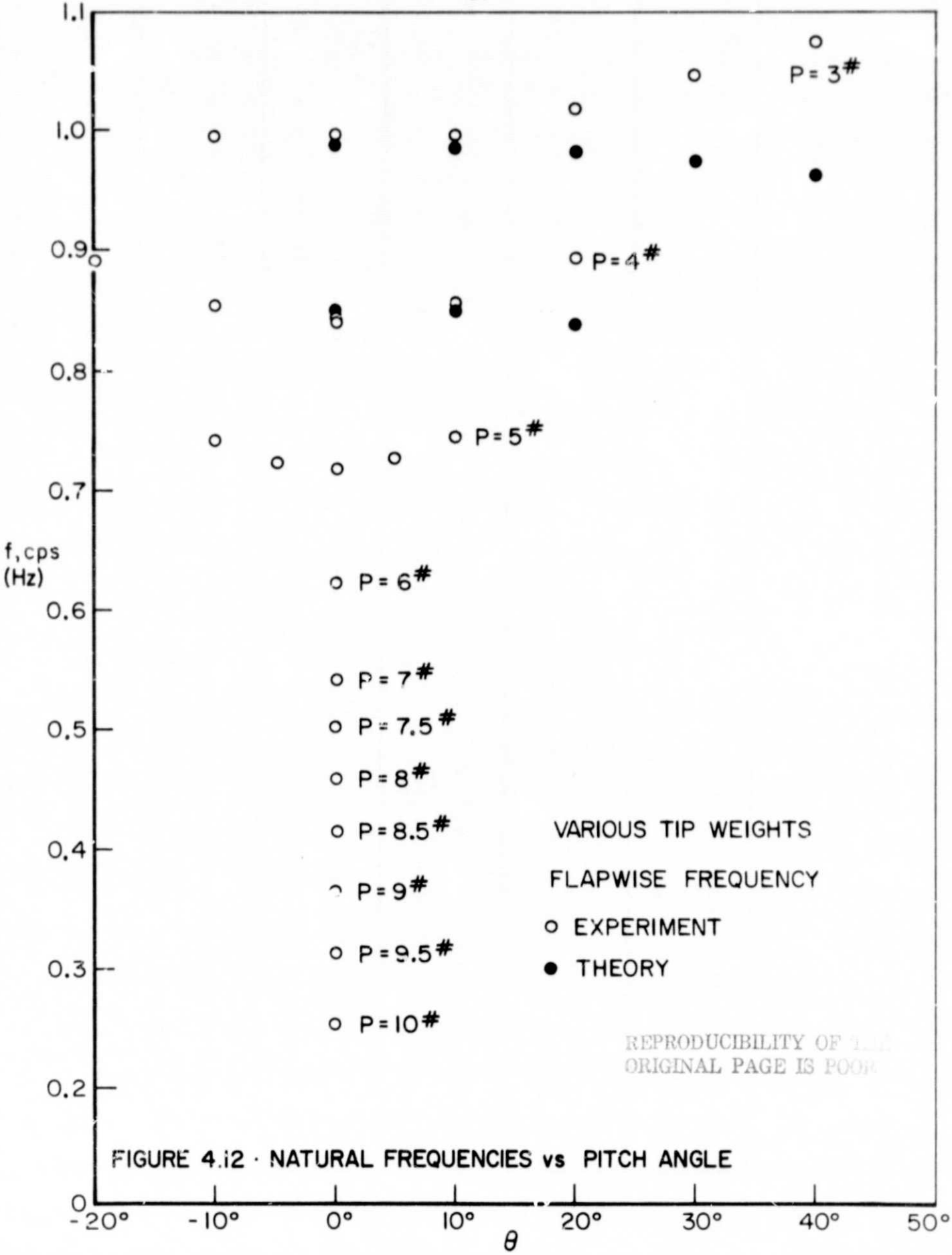

FIGURE 4.12 · NATURAL FREQUENCIES vs PITCH ANGLE

REPRODUCIBILITY OF THE
ORIGINAL PAGE IS POOR

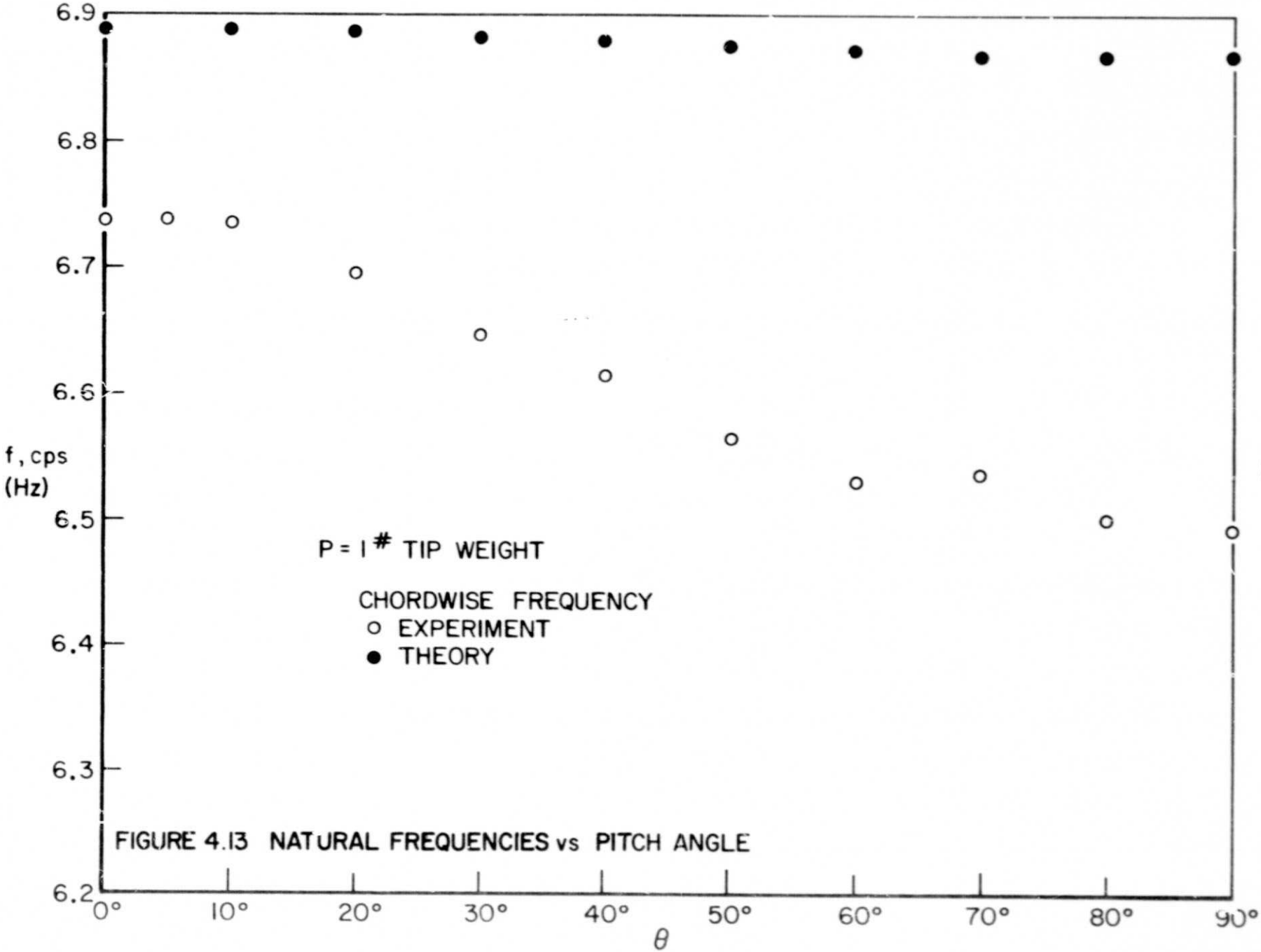

FIGURE 4.13 NATURAL FREQUENCIES vs PITCH ANGLE

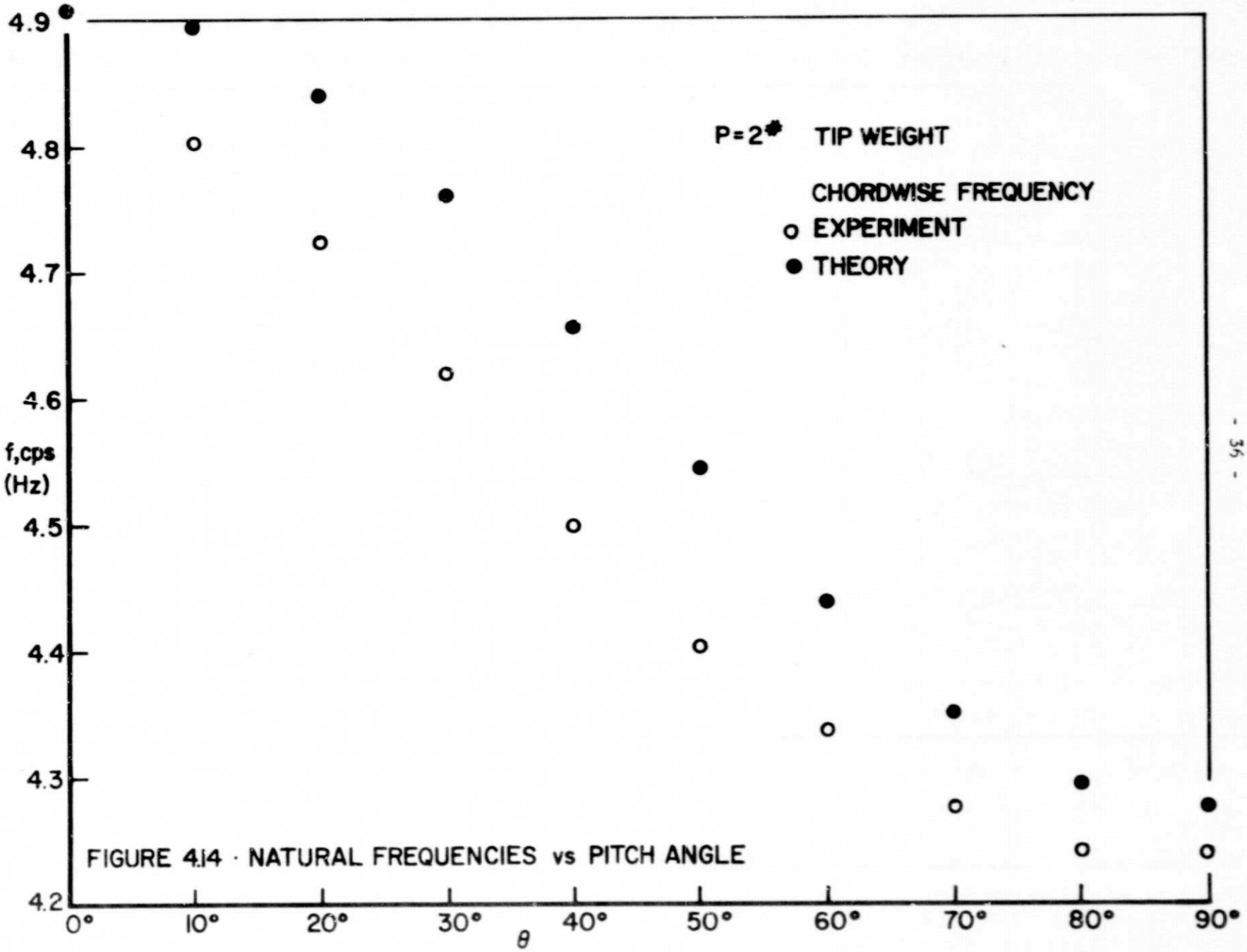

FIGURE 4.14 · NATURAL FREQUENCIES vs PITCH ANGLE

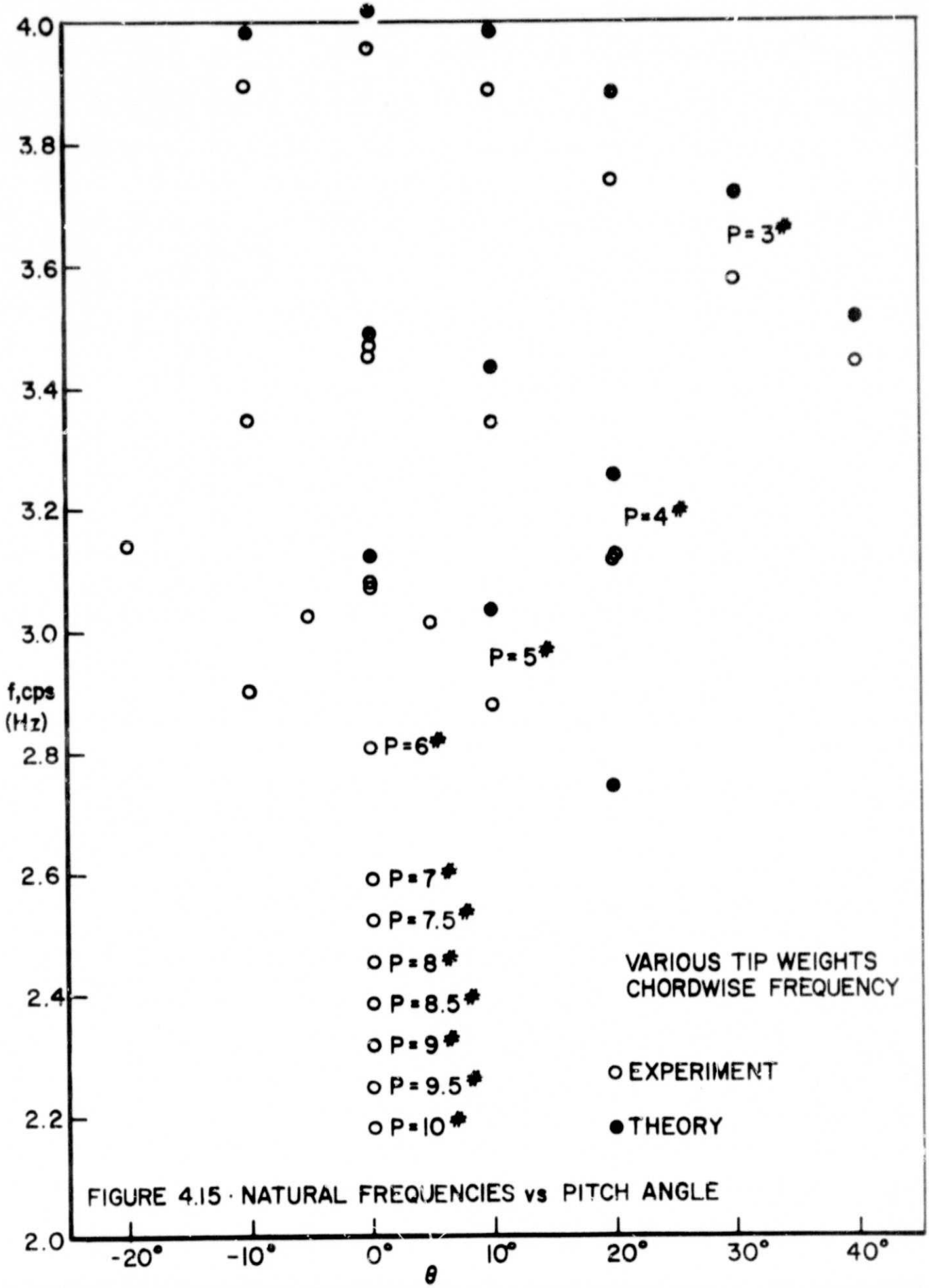

FIGURE 4.15 · NATURAL FREQUENCIES vs PITCH ANGLE

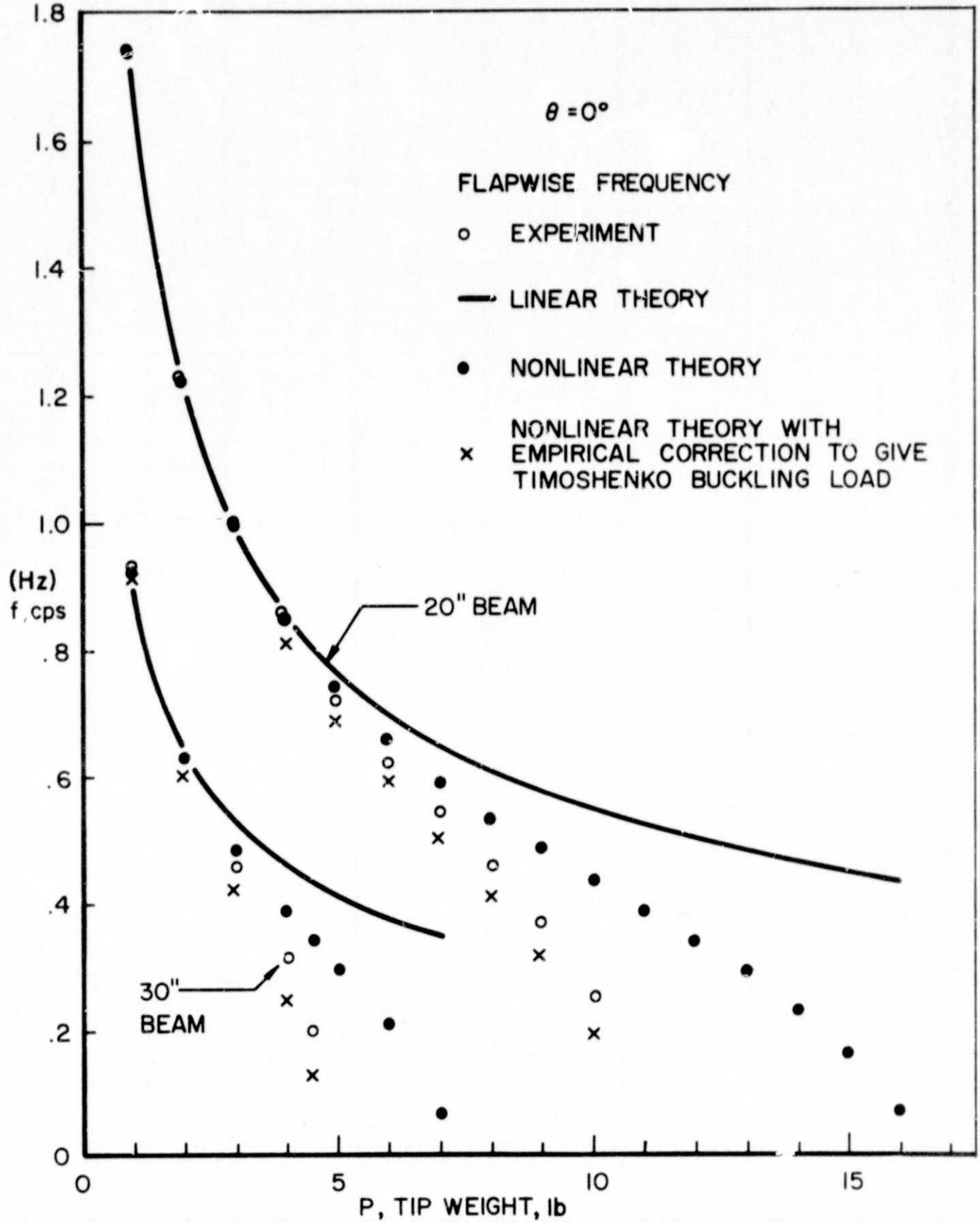

FIGURE 4.16 · NATURAL FREQUENCIES vs TIP WEIGHT

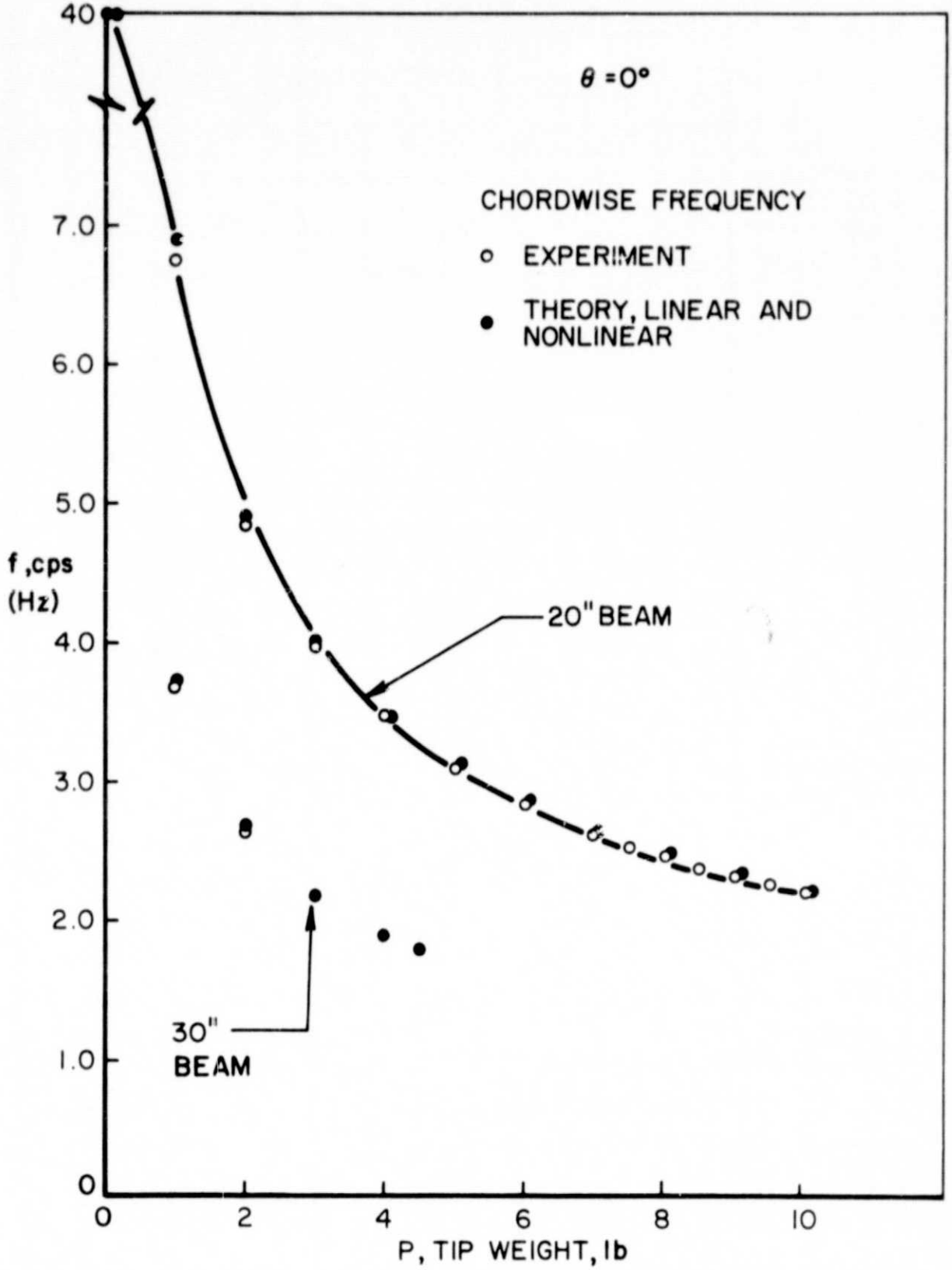

FIGURE 4.17 · NATURAL FREQUENCIES vs TIP WEIGHT

TABLE I

Test S1 : **Blade Frequency Experiments using Aluminum Beam**

Blade Radius and Cross-section: Radius = 20", Width = 1/2", Thickness = 1/8".

Run Number	Blade Tip Load (pounds)	Pitch Angle (Degrees)	Chordwise Frequency (Hertz)	Flapwise Frequency (Hertz)
1	1	0	6.738	-
2	1	0	-	1.734
3	1	5	6.738	-
4	1	5	-	1.734
5	1	-5	6.752	-
6	1	-5	-	1.734
7	1	10	6.737	-
8	1	10	-	1.739
9	1	20	6.698	-
10	1	20	-	1.742
11	1	30	6.648	-
12	1	30	-	1.748
13	1	40	6.616	-
14	1	40	-	1.753
15	1	50	6.565	-
16	1	50	-	1.763
17	1	60	6.531	-
18	1	60	-	1.767
19	1	70	6.540	-
20	1	80	6.503	-

TABLE I

Test 51 : Blade Frequency Experiments using Aluminum Beam

Blade Radius and Cross-section: Radius = 20", Width = 1/2", Thickness = 1/8".

Run Number	Blade Tip Load (pounds)	Pitch Angle (Degrees)	Chordwise Frequency (Hertz)	Flapwise Frequency (Hertz)
21	1	80	-	1.773
22	1	90	6.492	-
23	1	90	-	1.775
24	1	100	6.485	-
25	1	100	-	1.778
26	1	0	6.742	-
27	1	0	-	1.734
28	1	-10	6.742	-
29	1	-10	-	1.733
30	2	-10	4.810	-
31	2	0	4.834	-
32	2	0	-	1.226
33	2	10	4.802	-
34	2	10	-	1.230
35	2	20	4.724	-
36	2	20	-	1.241
37	2	30	4.620	-
38	2	30	-	1.260
41	2	40	-	1.276
42	2	40	-	1.277

REPRODUCIBILITY OF THE
ORIGINAL PAGE IS POOR

TABLE I

Test 5k Blade Frequency Experiments using Aluminum Beam

Blade Radius and Cross-section: Radius = 20", Width = 1/2", Thickness = 1/8".

Run Number	Blade Tip Load (pounds)	Pitch Angle (Degrees)	Chordwise Frequency (Hertz)	Flapwise Frequency (Hertz)
43	2	40	4.499	-
44	2	50	4.405	-
45	2	50	-	1.298
46	2	60	4.337	-
47	2	60	-	1.312
48	2	70	4.276	-
49	2	70	4.280	-
50	2	70	-	1.322
51	2	80	4.242	-
52	2	80	-	1.331
53	2	90	4.243	-
54	2	90	-	1.335
55	2	100	4.243	-
56	2	100	-	1.335
57	2	0	4.832	-
58	2	0	-	1.227
59	3	0	3.954	-
60	3	0	-	0.998
61	3	10	3.887	-
62	3	10	-	0.996

TABLE I

Test 51: Blade Frequency Experiments using Aluminum Beam

Blade Radius and Cross-section: Radius = 20", Width = 1/2", Thickness = 1/8".

Run Number	Blade Tip Load (pounds)	Pitch Angle (Degrees)	Chordwise Frequency (Hertz)	Flapwise Frequency (Hertz)
63	3	20	3.739	-
64	3	20	-	1.019
65	3	30	3.578	-
66	3	30	3.578	-
67	3	30	-	1.046
68	3	40	3.438	-
69	3	40	-	1.075
70	3	-10	3.896	-
71	3	-10	-	0.994
72	4	0	3.472	-
73	4	0	-	0.846
74	4	-20	3.139	-
75	4	-20	-	0.892
76	4	-10	3.348	-
77	4	-10	-	0.855
78	4	0	3.455	-
79	4	0	-	0.843
80	4	10	3.341	-
81	4	10	-	0.857
82	4	20	3.121	-

TABLE I

Test 51: Blade Frequency Experiments using Aluminum Beam

Blade Radius and Cross-section: Radius = 20", Width = 1/2", Thickness = 1/8".

Run Number	Blade Tip Load (pounds)	Pitch Angle (Degrees)	Chordwise Frequency (Hertz)	Flapwise Frequency (Hertz)
83	4	20	-	0.893
84	4	20	3.112	-
85	5	0	3.079	-
86	5	0	-	0.720
87	5	-10	2.902	-
88	5	-10	-	0.743
89	5	-5	3.026	-
90	5	-5	-	0.725
91	5	0	3.072	-
92	5	0	-	0.717
93	5	5	3.013	-
94	5	5	-	0.729
95	5	10	2.877	-
96	5	10	-	0.745
97	6	0	2.811	-
98	6	0	2.816	-
99	6	0	-	0.623
100	6	0	-	0.625
101	7	0	2.614	-
102	7	0	2.616	

TABLE I

Test 51: Blade Frequency Experiments using Aluminum Beam

Blade Radius and Cross-section: Radius = 20", Width = 1/2", Thickness = 1/8".

Run Number	Blade Tip Load (pounds)	Pitch Angle (Degrees)	Chordwise Frequency (Hertz)	Flapwise Frequency (Hertz)
103	7	0		0.543
104	7	0		0.543
105	0	0	41.143	10.154
106	0	0		10.152
107	0	0		10.143
108	7	0	2.616	-
109	7	0	-	0.543
110	7.5	0	2.531	-
111	7.5	0	-	0.502
112	8	0	2.446	-
113	8	0	-	0.457
114	8.5	0	2.374	-
115	8.5	0	-	0.413
116	9	0	2.299	-
117	9	0	2.311	-
118	9	0	-	0.365
119	9.5	0	2.251	-
120	9.5	0	-	0.312

REPRODUCIBILITY OF THE
ORIGINAL PAGE IS POOR

TABLE II

Test 52 : **Blade Frequency Experiments using Aluminum Beam**

Blade Radius and Cross-section: Radius 30", Width = 1/2", Thickness = 1/8"

Run Number	Blade Tip Load (pounds)	Pitch Angle (Degrees)	Chordwise Frequency (Hertz)	Flapwise Frequency (Hertz)
1	1	0	3.689	-
2	1	0	-	0.932
3	1	90	3.143	
4	1	90	-	1.035
5	0	0	17.217	-
6	0	0	17.213	-
7	0	0	17.171	-
8	0	0	17.174	-
9	0	0	-	4.475
10	0	0	-	4.607
11	0	0	-	4.490
12	1	0	3.647	-
13	1	0	3.662	-
14	1	10	3.617	-
15	1	10	-	0.935
16	1	20	3.541	-
17	1	20	-	0.945
18	1	30	3.448	-
19	1	30	-	0.960
20	1	35	3.394	-

TABLE II

Test 52: **Blade Frequency Experiments using Aluminum Beam**

Blade Radius and Cross-section: Radius = 30", Width = 1/2", Thickness = 1/8"

Run Number	Blade Tip Load (pounds)	Pitch Angle (Degrees)	Chordwise Frequency (Hertz)	Flapwise Frequency (Hertz)
21	1	40	3.354	-
22	1	40	-	0.979
23	1	50	3.277	-
24	1	50	-	0.997
25	1	60	3.215	-
26	1	60	-	1.012
27	1	70	3.175	-
28	1	70	-	1.023
29	1	80	3.145	-
30	1	80	-	1.032
31	1	90	3.138	-
32	1	90	-	1.033
33	1	105	3.155	-
34	1	105	-	1.029
35	1	-105	3.138	-
36	1	-105	-	1.033
37	1	-90	3.122	-
38	1	-90	3.120	-
39	1	-90	-	1.034
40	1	-75	3.135	-

TABLE II

Test 52 : **Blade Frequency Experiments using Aluminum Beam**

Blade Radius and Cross-section: Radius = 30", Width = 1/2", Thickness = 1/8"

Run Number	Blade Tip Load (pounds)	Pitch Angle (Degrees)	Chordwise Frequency (Hertz)	Flapwise Frequency (Hertz)
41	1	-75		1.028
42	1	-60	3.199	-
43	1	-60	-	1.011
44	1	-45	3.298	-
45	1	-45	-	0.990
46	1	-30	3.443	-
47	1	-30		0.961
48	1	-15	3.591	-
49	1	-15		0.939
50	1	0	3.674	-
51	1	0		0.928
52	2	0	2.629	-
53	2	0	-	0.632
54	2	5	2.559	-
55	2	5	-	0.636
56	2	10	2.517	-
57	2	10	-	0.648
58	2	15	2.424	-
59	2	15	-	0.664
60	2	20	2.317	-

TABLE II

Test 52: Blade Frequency Experiments using Aluminum Beam

Blade Radius and Cross-section: Radius = 30", Width = 1/2", Thickness = 1/8"

Run Number	Blade Tip Load (pounds)	Pitch Angle (Degrees)	Chordwise Frequency (Hertz)	Flapwise Frequency (Hertz)
61	2	20	-	0.683
62	2	0	2.637	-
63	2	0	-	0.631
64	2	-10	2.517	-
65	2	-10	-	0.648
66	2	-20	2.315	-
67	2	-20	-	0.682
68	2	25	2.232	-
69	2	25	-	0.706
70	3	0	2.162	-
71	3	0	-	0.462
72	3	5	2.043	-
73	3	5	-	0.478
74	3	10	1.863	-
75	3	10	-	0.515
76	3	15	1.731	-
77	3	15	-	0.553
78	3	-15	1.723	-
79	3	-15	-	0.555
80	3	-10	1.862	-

REPRODUCIBILITY OF THE
ORIGINAL PAGE IS POOR

TABLE II

Test 52: **Blade Frequency Experiments using Aluminum Beam**

Blade Radius and Cross-section: Radius = 30", Width = 1/2", Thickness = 1/8".

Run Number	Blade Tip Load (pounds)	Pitch Angle (Degrees)	Chordwise Frequency (Hertz)	Flapwise Frequency (Hertz)
81	3	-10	-	0.514
82	3	0	2.161	-
83	3	0	-	0.461
84	4	0	1.900	-
85	4	0	-	0.317
86	4	5	1.538	-
87	4	5	-	0.398
88	4	-5	1.558	-
89	4	-5	1.559	
90	4	-5		0.391
97	4.5	0	1.784	
98	4.5	0	-	0.199
99	4.5	0	-	0.199
100	0	0	17.207	-
101	0	0	17.258	-
102	0	0	-	4.464

REFERENCES

1. Hodges, D. H., "Nonlinear Bending and Torsion Equations for Rotating Beams with Application to Linear Stability of Hingeless Rotors", Ph.D. Thesis, Stanford University, December 1972.
2. Hodges, D. H. and Dowell, E. H., "Nonlinear Equations of Motion for the Elastic Bending and Torsion of Twisted Nonuniform Rotor Blades", NASA TN D-7818.
3. Timoshenko, S. P., and Gere, J. M., "Theory of Elastic Stability", McGraw-Hill, New York, 1961.